Quantification of transient signals in multiple collector inductively coupled plasma mass spectrometry: Accurate lead isotope ratio determination by laser ablation of individual fluid inclusions

Thomas Pettke[1, ‡], Felix Oberli[1], Andreas Audétat[2], Uwe Wiechert[1,¤], Caroline R. Harris[1,*], and Christoph A. Heinrich[1]

1 Institute of Geochemistry and Petrology, ETH Zurich, Clausiusstrasse 25, CH-8092 Zurich, Switzerland

2 Bayerisches Geoinstitut, Universität Bayreuth, D-95440 Bayreuth, Germany

Present addresses:

‡ Institute of Geological Sciences, University of Bern, Baltzerstrasse 1+3, CH-3012 Bern, Switzerland

¤ Institut für Geologische Wissenschaften, Freie Universität Berlin, D-12249 Berlin, Germany

* Geological and Environmental Sciences, Stanford University, 367 Panama St, Stanford, California 94305, U.S.A.

Corresponding author: Thomas Pettke Pettke@geo.unibe.ch

Table of contents entry:

We present a detailed evaluation of techniques to obtaining highly accurate isotope ratios from fast transient signals recorded by MC-ICP-MS

Please cite as:

Pettke, T., Oberli, F., Audetat, A., Wiechert, U., Harris, C. R., and Heinrich, C. A., 2011. Quantification of transient signals in multiple collector inductively coupled plasma mass spectrometry: accurate lead isotope ratio determination by laser ablation of individual fluid inclusions. Journal of Analytical Atomic Spectrometry 26, 475-492. doi: 10.1039/C0JA00140F

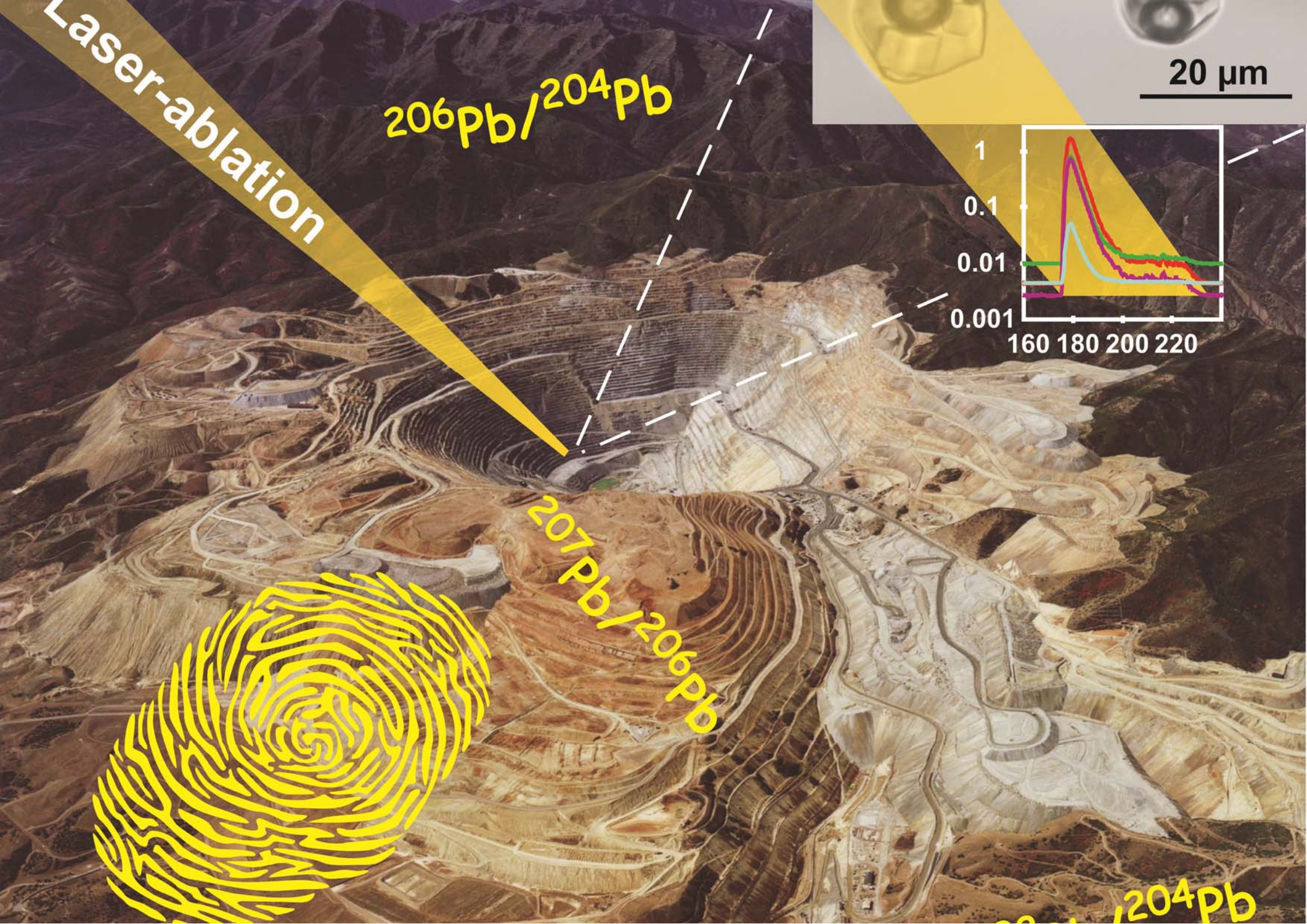
Laser-ablation
$^{206}Pb/^{204}Pb$
$^{207}Pb/^{206}Pb$
$^{208}Pb/^{204}Pb$
20 µm
1
0.1
0.01
0.001
160 180 200 220

Summary

This work establishes the analytical protocol for accurate Pb isotopic analysis of fast transient signals by multiple-collector ICP-MS instruments. Individual synthetic fluid inclusions of known Pb and Tl isotopic compositions (dissolved SRM 981 with or without SRM 997 from NIST, enclosed in quartz by a hydrothermal crack annealing technique) were liberated by 193 nm UV laser ablation (LA). Data were recorded on Faraday detectors, for which correction schemes for bias in amplifier response ("*tau* correction") are presented and evaluated. *tau*-corrected Pb isotope data data reveal LA-induced isotope fractionation amounting to ~0.5 % a.m.u.$^{-1}$ for Pb isotopes over the course of an entire fluid inclusion ablation.

Instrumental mass bias correction was effected within-run using Tl provided by the fluid inclusion itself or admixed to the ablation aerosol via desolvated nebulization. Isotope ratios derived from the transient signals were either based on individual readings or on bulk signal integration, of which the latter produces significantly more accurate data.

The external precision achieved by ablating SRM610 glass with a 60 µm beam is ± 0.011 % (2SD, relative) for $^{208}Pb/^{206}Pb$ and $^{207}Pb/^{206}Pb$ ratios and ± 0.032 % for Pb isotope ratios normalized to mass 204 (n=18). Inclusion-to-inclusion reproducibilities (n=11; ~0.1 ng Pb per inclusion) are ±0.05 % (2SD; $^{208}Pb/^{206}Pb$ and $^{207}Pb/^{206}Pb$) and ±0.13 % ($^{20X}Pb/^{204}Pb$), respectively; inclusions containing as little as 0.005 ng Pb returned ± 0.1 % and ±0.8 %. These results are accurate as demonstrated by analysis of synthetic fluid inclusions containing SRM 981 Pb. The analytical protocol presented here for measuring isotope ratios on minute analyte quantities by multiple-collector ICP-MS in fast transient signal mode has great potential for applications to geochemical, archaeological, environmental and possibly biochemical problems.

Introduction

Laser ablation inductively coupled plasma mass spectrometry (LA-ICP-MS) has demonstrated capabilities in the chemical analysis of solids (*e.g.,* Sylvester[1]) and even heterogeneous inclusions in them, such as fluid or melt inclusions in minerals (*e.g.,* Günther et al.[2]; Audétat et al.[3]; Halter et al.[4]; Heinrich et al.[5]; Pettke et al.[6]; Allan et al.[7]; Spandler et al.[8]; Pettke[9]). Latest studies have explored the potential of the LA-ICP-MS technique for *in-situ* dating and for the determination of isotope ratios in geochemical, environmental and biological studies. Successful examples of geochemical applications using various isotope systems at adequate precision are rapidly accumulating (*e.g.,* Walder et al.[10]; Hirata[11]; Hirata et al.[12]; Paul et al.[13]; Kosler et al.[14], Jackson and Hart[15]; Paton et al.[16]; Gounelle et al.[17]; Fietzke et al.[18]; Cottle et al.[19]; Woodhead et al.[20]). Here, we develop the LA-ICP-MS method for using Pb isotopes to trace fluid provenance and migration in ore-forming geological systems[21].

To obtain accurate and precise isotope ratios by ICP-MS it is crucial to properly correct for mass dependent fractionation and other signal bias occurring at various stages, from the site of laser ablation to that of ion detection. Among possible sources of fractionation, instrumental mass bias is commonly considered to be most prominent. Its nature and possible correction strategies have been investigated in great detail for multiple-collector (MC)-ICP-MS instruments (for the Pb system, see Rehkämper and Mezger[22]; Woodhead[23]; Thirlwall[24], Albarède et al.[25]; Baxter et al.[26]). Surprisingly little is known, however, about the nature and extent of isotopic fractionation at the laser ablation site (*e.g.,* Jackson and Günther[27], Kuhn et al.[28]). Thus, the question has remained whether instrumental mass bias at the plasma interface is the dominant, if not the only, factor contributing to the deviation of measured isotope ratios from true values, or whether aerosol generation at the LA site, transport processes and signal recording characteristics may also contribute to the overall bias in isotope ratios encountered.

Instrumental mass bias is dominated by kinetic and space charge effects at the ICP-MS interface. A common correction method requires a pair of non-radiogenic isotopes characterized by an invariant isotopic ratio in nature, ideally from the same element (*e.g.,* Nd, Sr, Hf). This method, originally developed for TIMS isotope analysis, has since successfully been implemented by the ICP-MS community (see reviews by Halliday et al.[29]; Albarède et al.[25]). Some elements, most importantly Pb, do not possess such an invariant isotope pair, however. At an early stage, Longerich et al.[30] therefore proposed to admix Tl, a neighbouring mass element with an invariant isotopic ratio, to the sample and use it for mass bias correction of Pb, assuming that instrumental mass bias is a sole function of mass. As the analytical precision on ICP-MS isotope ratio measurements has improved, notably through the introduction and further development of MC-ICP-MS instruments and double- or triple-spike (enriched isotope) techniques, it became clear that inter-elemental mass bias in ICP-MS instruments is not merely a function of mass (*e.g.,* Rehkämper and Mezger[22]; Thirlwall[24];

Woodhead[23]). Consequently, it was claimed[24,31] that the use of Tl for within-run correction of mass bias would result in Pb isotope data that would be less accurate than those obtained by double- or triple-spike techniques. However, simple modifications to existing mass bias correction protocols using Tl allowed Woodhead[23] to produce MC-ICP-MS Pb isotope data matching double-spike TIMS results in accuracy. An elegant redesign of the mass bias correction protocol by Baxter et al.[26] achieves an equivalent level of accuracy for within-run Tl based correction.

In contrast to solution analysis of Pb, where Tl is directly admixed to the sample, the LA-ICP-MS method requires a different approach. Ideally, the sample to be analysed contains naturally occurring, non-fractionated Tl at sufficient concentration to allow for within-run Tl-based instrumental mass bias correction, but this is almost never the case (e.g., Audétat et al.[32]). Alternative methods for mass bias correction include (i) admixture of Tl or Pb-spike aerosol, produced by nebulisation of a Tl standard or Pb spike solution, to the LA aerosol before it enters the ICP, or (ii) bracketing standardization. Matrix matching has been claimed[25] to be vital for highly accurate isotope ratio measurements by bracketing standardization. This approach, widely used for “simple” matrices, is inappropriate for fluid inclusions, because Pb is partly dissolved in the aqueous phase and may partly reside in salt precipitates within the inclusions that are hosted by quartz.

In this study, we document the procedures developed for Pb isotopic analysis of fast transient signals as produced by laser ablation of fluid inclusions in minerals, following a first feasibility test[33]. Our experimental approach is based on fluid inclusion standards prepared with known Pb and Tl isotopic compositions in order to explore different schemes for mass bias correction and possibly discriminate between fractionation occurring at the LA site and in the ICP, respectively. We show that isotope fractionation at the LA site poses no limitation to accuracy provided that fluid inclusion ablation is well controlled. We identify isotope ratio bias related to bias in amplifier response and provide two approaches to correct for these. We explore different signal integration schemes and conclude that the bulk signal integration method provides the most accurate data. Within-run mass bias correction by the methods of both Woodhead[23] and Baxter et al.[26] produces accurate Pb isotope data from individual fluid inclusions at precision levels (both within-inclusion and inclusion-to-inclusion), which are only a factor of about five poorer than the best external precision achieved for the NIST SRM 610 standard. An application of our techniques to two assemblages of natural fluid inclusions shows analytical precisions even superior to those obtained on the fluid inclusion standards and thus demonstrates the great potential of this technique for accurate isotope ratio determinations of minute sample amounts recorded in transient signal mode.

Methods

Synthetic fluid inclusion standards

Two sets of synthetic fluid inclusion standards were produced, one containing only Pb (SRM 981) and the other prepared with both Pb and Tl (SRM 981 and SRM 997) in an aqueous NaCl-KCl solution of *ca.* 17 wt% bulk salinity (Table 1). A pre-fractured, pure quartz rod (3 * 10 mm) or a stack of etched quartz plates was loaded with SiO_2 glass and standard solutions into gold capsules closed by welding. Inclusions were formed at 700 °C / 180 MPa over 144 h in cold-seal pressure vessels pressurized with water. Oxygen fugacity was constrained near Ni-NiO by the steel of the pressure vessel and a nickel filler rod. Equal weights of the filled gold capsules before and after the experiment demonstrate that no matter was lost or gained except probably small amounts of hydrogen. Doubly polished thick sections were prepared from the recovered quartz samples. Product inclusions have a bulk density of approximately 0.7 - 0.8 g cm^{-3} and average sizes of 5-30 µm in diameter, with a few reaching 80 µm. Interestingly, inclusions containing only Pb (Pb-only inclusions) were all rather flat and small while those containing Pb and Tl (Pb-Tl inclusions) formed larger, isometric inclusions (Fig. 1). Repeated runs under varying experimental conditions did not notably improve size and shape of the Pb-only inclusions.

Lead and Tl contents of the synthetic fluid inclusions were determined by LA-ICP-Quadrupole-MS (QMS) at ETH Zurich following methods reviewed by Heinrich et al.[5] with instrumental setup and tuning conditions detailed in Pettke et al.[6]. Resulting concentrations (Table 1) suggest loss of Pb and Tl of up to 20% from the solution prior to fluid inclusion formation during the experiment. This could be either due to precipitation of Pb and Tl from the stock solution prior to loading (indeed, a few microscopic particles could be observed in the stock solution at the time of capsule loading), or result from loss of Pb and possibly Tl to the Au capsule wall prior to inclusion formation. Considering the Pb and Tl concentrations as measured in the synthetic fluid inclusions (Table 1) an egg-shaped Pb-Tl fluid inclusion with longest diameter of 30 µm, the amount of Pb available for analysis is of the order of 0.02 ng. This is considerably less than the amounts consumed for precise MC-ICP-MS isotope analysis of Pb in solution mode using Faraday detectors (isotopic ratios of ± 0.01 % external precision can be obtained on amounts of Pb as low as *ca.* 5-10 ng[31]). Note that our largest-diameter Pb-only inclusions contain considerably less Pb because of their flatter and more irregular shape and, hence, lower total volume (Fig. 1). Interestingly, Pb-Tl fluid inclusion measurements by both QMS and MC-ICP-MS reveal non-proportional signals for Tl and Pb (*e.g.,* Fig. 2A), indicating that Pb and Tl are not localized in the same inclusion phase at room temperature. Variable bulk fluid inclusion Pb/Tl intensity ratios measured on both MC-ICP-MS and QMS instruments furthermore suggest heterogeneous distribution of Pb and Tl in the product inclusions.

LA-MC-ICP-MS instrument details and analytical strategies

All LA-MC-ICP-MS Pb isotope analyses were performed at ETH Zurich using a GeoLas 200Q (Lambda Physik, Germany) laser system with computer-controlled sample stage connected to either a Nu Plasma or a Nu Plasma 1700 MC-ICP-MS instrument (Nu Instruments Ltd, Wrexham, UK). Table 2 summarizes the operating conditions for LA-ICP-MS analysis of Pb isotopes, plus the ranges in parameters explored during this study. An energy-homogenized laser beam profile with sufficient energy density on the sample surface (>15 J/cm^2) is essential for controlled ablation of fluid inclusions in quartz[5]. The first feasibility tests using a MC-ICP-MS instrument[33] achieved analytical precisions for individual inclusions considerably better than those reported for sequential signal recording using a quadrupole instrument. The latter technique is hampered by limitations in representative recording of fast transient signals[34] and poor duty cycle, whereas for simultaneous ion detection the duty cycle is nearly an order of magnitude larger for the isotope sequence analysed here (Table 2). Therefore, single-collector instruments were not further evaluated in this study.

Before the helium stream transporting the aerosol from the LA chamber enters the torch, an Ar-based aerosol is admixed from a desolvator aspirating an ultrapure ~1% HNO_3 solution containing either Tl or no metal. The MC-ICP-MS instruments were optimized daily for maximum sensitivity, perfect peak flatness and coincidence by admixing a desolvated aerosol generated from a 30 ng g^{-1} Pb - 32 ng g^{-1} Tl solution to the He flow from the LA chamber. Minor re-tuning was then performed using an aerosol produced from SRM 610 laser ablation in line scan mode (Table 2), while aspirating a pure 1% HNO_3 solution. Optimization with Ar alone (i.e., without a He flow from the LA chamber) is inadequate because the focusing properties of the MC-ICP-MS instruments are rather sensitive to gas composition and flow rate.

The analyses were performed in static time-resolved mode using modified instrument control and data acquisition software, collecting ^{200}Hg-^{202}Hg-^{203}Tl-^{204}(Hg,Pb)-^{205}Tl-^{206}Pb-^{207}Pb-^{208}Pb simultaneously in 8 Faraday cups calibrated daily for their preamplifier gains. All experiments were performed with the same Tl standard solution. However, care was taken not to expose the solution to light during storage in order to avoid variations in Tl speciation potentially leading to mass fractionation effects during the desolvating process[35]. The signals at masses 200-208 were recorded at 0.2 s integration intervals. For the measurement of samples containing both Pb and Tl (SRM 610 glass and Pb-Tl inclusions), the LA signal was acquired after having collected the background on peak for at least 50 seconds (laser pulsing turned off), while aspirating a pure 1% HNO_3 solution (Figs. 2A, B). For Pb-only inclusions, the background was acquired in the same way, then the Tl-solution was aspirated, and once the Tl signal was stable, LA was started, superimposing the fluid inclusion signal on the Tl signal from the desolvating unit (Fig. 2C). Sections for background and signal processing were carefully chosen by re-evaluation of each measurement off-line using criteria detailed below. Mass bias correction was exclusively done in within-run mode. Optimum Pb

sensitivities determined on desolvated Pb-Tl standard solutions in this mixed Ar-He plasma mode were about 250 V (Nu Plasma 1700) and 180 V (Nu Plasma) relative to a Pb concentration of 1 μg per g of solution, at uptake rates of approx. 80 μl/minute.

LA conditions and interface setup were optimized by a series of tests at different experimental conditions using SRM 610 glass. The final parameters derived from these experiments (Table 2) were then applied to fluid inclusion analysis. Each set of fluid inclusion analyses was bracketed by 2-3 measurements on SRM 610 glass in order to monitor machine performance. Mass bias relationships between Pb and Tl were established based on the total set of SRM 610 measurements acquired over the duration of the project and then applied to the individual fluid inclusion analyses based on measured Tl aspirated through a desolvating unit or contained by the inclusions. The SRM 610 standard measurements were always done in line-scan mode (1 μm/s transport rate, 60 μm spot size, 6 Hz pulse repetition rate, 90 s signal recording), after having ensured that single-spot and line-scan mode give the same Pb isotopic results at >2 Hz laser repetition rate.

Data reduction

Transient signal data reduction was done by revisiting the individually stored readings using modified Nu Instruments software (steps 1-4), followed by off-line evaluation on Excel spreadsheets (step 5). (1) Individual raw readings were corrected for amplifier response effects (referred to as *tau* correction and outlined in detail below), since the original instrument software does not provide for appropriate correction of fast transient signals. (2) The readings from selected background sections were averaged and used for baseline correction of individual, simultaneously acquired 0.2 s readings from selected signal sections, followed by (3) an interference correction for Hg contribution to mass 204 based on ^{202}Hg. (4) Two different approaches to derive mean isotopic ratios for an individual fluid inclusion were explored in our study. In a first approach named the “individual reading integration method”, isotopic ratios were calculated for individual background- and interference-corrected 0.2 s signal readings, filtered by a one-pass 2-sigma outlier removal test, then averaged and finally (5) corrected off-line for mass bias (all data reported in Tables A1 and A2 have been reduced this way). In a second approach named “bulk signal integration method”, the background-corrected signal intensities were summed up, and further data reduction then carried out on this single set of integrated intensity readings.

The Hg interference correction on mass 204 in step 3 was based on the measured ^{202}Hg beam and a ^{202}Hg/^{204}Hg ratio of 4.32, adjusted to the fractionated state by use of an exponential mass bias coefficient derived from the measured ^{205}Tl/^{203}Tl ratio and its common value of 2.3871[36]. Final mass-bias corrected ^{20x}Pb/^{204}Pb ratios do not correlate with ^{202}Hg/Pb$_{(total)}$, demonstrating successful removal of Hg interference. Owing to low beam intensities on Faraday cups, the measured ^{202}Hg/^{200}Hg isotope ratio could not be measured precisely enough to directly derive a fractionation coefficient for Hg. The Hg intensity of the gas background, too, was insufficient for determining a precise Hg-specific mass bias (*cf.*

Paul et al.[13]). As will be shown below, correction for ^{204}Hg interference alone based on ^{202}Hg produces sufficiently accurate results and thus demonstrates that other potential interferences (*e.g.,* WO^+, REE argides) are not relevant at the level of our external analytical precision.

Mass bias correction in step 5 was effected using the refined empirical procedure of Baxter et al.[26] for obtaining mass-bias corrected isotope ratios with minimized uncertainty magnification. This procedure establishes *lnTl - lnPb* relationships that are machine- and isotope ratio specific. It uses the linear relationship in *ln-ln* space between the mass biases of the internal standard (Tl) and the target (Pb) isotope ratios measured in the sample (*i.e.*, the fluid inclusions) and relates it to that established experimentally on the reference material (SRM 610 glass here). All robust SRM 610 data acquired during several years since setting up the LA-ICP-MS fluid inclusion analytical method were used to define such *lnTl - lnPb* relationships. These long-term, well-defined average fractionation trends were then employed for mass bias correction because the spread in *lnTl - lnPb* values from individual analytical sessions was always too small to derive well-defined linear regression parameters. During methods development, significant modifications of the ICP-MS front end such as the use of different types of sampler and skimmer cones and reduction of interface pressure to the values reported in Table 2 were implemented. This caused a considerable range in instrumental mass bias, thus enhancing the definition of the *lnTl - lnPb* relationships. Individual fluid inclusion analyses were thus corrected for mass bias using the within-run measured ^{205}Tl/^{203}Tl isotope ratio and the Baxter et al.[26] approach, after ensuring that the bracketing SRM 610 measurements were consistent with our long-term *lnTl - lnPb* relationships. Previously, Woodhead[23] derived a *fTl - fPb* relationship, the use of which returned identical results (within uncertainties) for our data set. Resulting fluid inclusion Pb isotope ratios are accurate at the external precisions achieved by the LA-MC-ICP-MS analyses (see below).

Results and discussion

SRM 610 data

All data sets obtained on the SRM 610 standard glass and used for establishing the mass-bias correction parameters are listed in Table A1 (electronic appendix). The data include homogeneity tests on SRM 610, variations in laser pulse repetition rate and laser energy for single spot ablation and scanning experiments as well as results on standard runs interspersed with the fluid inclusion analyses. Acquired during several years, these data display remarkably correlated trends with few outliers. Outliers in $f_{208Pb/206Pb}$ and $f_{207Pb/206Pb}$ vs. f_{Tl} plots (not shown) are analyses with Pb/Tl intensity ratios as high as 34, well above Pb/Tl = 6 to 8 as commonly measured. These elevated Pb/Tl ratios identify zones in the SRM 610 glass characterized by variably enhanced loss of Tl during glass manufacture (*e.g.,* Eggins and Shelley[37]; Kent[38]), which also may have caused isotopic fractionation. Therefore, SRM 610 analyses with Pb/Tl intensity ratios >9 were discarded. This is a robust criterion, since

day-to-day variability in Pb/Tl intensity ratios that could result from differences in the daily tuning of the LA-ICP-MS instrument was only marginally larger than within-day variability.

The large SRM 610 dataset collected for this study allows evaluation of analytical precision at various scales, from internal (within-run) precision to that achieved during the entire methods development (Table A1). Analytical accuracy, on the other hand, cannot be evaluated from this data set as it serves as a base for the calibration of the unknown Pb isotope composition of the fluid inclusions. The external reproducibility of the mass-bias corrected isotope ratios achieved within one analytical session on Nu Plasma 1700 was *ca.* 110 ppm (2 SD, n=18) for $^{208}Pb/^{206}Pb$ and $^{207}Pb/^{206}Pb$ ratios, and 320 ppm for Pb isotope ratios relative to mass 204 (Table 3), the long-term external reproducibility being only slightly larger. The same uncertainties expressed as two standard errors of the mean of the 18 analyses of that session are 26 and 75 ppm, respectively. Our analytical reproducibility compares well with LA-MC-ICP-MS data reported elsewhere[39] for SRM 610 (see also Paul et al.[13]). The measurement session at Nu Plasma 1700 referred to (data from August 30, 2005; Table 3) included 3 ablation chamber loadings and lasted for about 13 hours. The amount of Pb consumed per line scan analysis is *ca.* 300-400 pg. The reduced precision on mass 204 is due to low beam intensities of 3.5-5.0 x 10^{-13} A, resulting in some correlation in $^{20x}Pb/^{204}Pb$ vs. $^{20y}Pb/^{204}Pb$ plots (Fig. 3A). This correlation cannot be due to inadequate mass bias correction, since other combinations of mass bias corrected isotope ratios (*e.g.,* $^{207}Pb/^{204}Pb$ vs. $^{208}Pb/^{206}Pb$, Fig. 3B) do not show such correlation and because the slope of the data array is indicative of error predominantly associated with the measurement of mass 204. Data obtained on Nu Plasma exhibit the same overall features but external precision is somewhat poorer (Table 3), partially owing to the lower sensitivity achieved for laser ablation using this instrument.

Woodhead[23] made use of matrix effects (variation in chemical purity of the analyte) to create sufficient spread in f_{Tl} - f_{Pb} to precisely define their functional relationship, but the invariant matrix of our reference material (SRM 610) did not allow for such an approach. Instead, we had to rely on variations of our interface configuration (*e.g.,* choice of cones and interface pressures) and operating conditions such as ablation chamber (He) and desolvator (Ar) gas flows during the course of this study. The observed variations in our f_{Tl} and f_{Pb} values are thus predominantly related to variations in the ion production and extraction processes, which are also influenced by daily ICP-MS optimization. It is remarkable indeed that for each instrument and Pb isotope ratio, a systematic f_{Tl} - f_{Pb} relationship can be maintained over several years in spite of substantial hardware modifications.

The effect of peak tailing interference on mass 204 from a large ^{205}Tl peak (*e.g.,* Thirlwall[24]) as could be obtained when admixing Tl via desolvated nebulisation during sample measurement is calculated to be insignificant in our case for measured Pb/Tl intensity ratios of 1 or higher, at the external reproducibility achieved in LA-ICP-MS mode. The abundance

sensitivities are approximately 1 - 2 * 10^{-6} for the Nu Plasma1700 and ~ 2 - 4 * 10^{-6} for the Nu Plasma instruments at mass 237.

Synthetic fluid inclusions

Data acquired during method testing reveal that it is important to control the ablation process of inclusions, in such a way that smooth signals conducive to accurate data integration are produced, rather than short signal spikes caused by “explosion” of the inclusion or breakage of the host quartz. The ablation process was therefore routinely monitored on a video screen. The best analyses were achieved for inclusions of up to *ca.* 50 µm largest diameter located 50-80 µm below sample surface, by enlarging the diameter of the pit in step-wise fashion to the final pit size *before* the inclusion was intersected (Fig. 2C; *straight ablation technique*[9]). A step-wise enlargement of the pit *during* inclusion ablation (*step-wise opening technique*[2]; Fig. 2B) was not beneficial because the overall signal-to-noise ratio decreases when the same total amount of ions available from the inclusion is analyzed over a longer period and because of very rapid changes in signal intensity (see below). This holds in particular for mass 204, where an unduly slow ablation process can yield uncertainties which render the data useless.

Isotope ratio evolution trends during an individual inclusion analysis

Inspection of the time-resolved, background-corrected analyte intensities measured at 0.2 s reading intervals reveals that isotope ratios evolve with progressive ablation of an individual fluid inclusion. For Pb-Tl inclusions, where Pb and Tl are both provided by the fluid inclusions, both Pb and Tl show evolving isotope ratios (Fig. 4 A, B), spanning several percent, whereas $^{205}Tl/^{203}Tl$ does not evolve across the fluid inclusion ablation when Tl is admixed through desolvating nebulisation as for Pb-only inclusions (Fig. 4 C, D). In detail, raw $^{208}Pb/^{206}Pb$ ratios become lighter while $^{205}Tl/^{203}Tl$ ratios become heavier with progressive ablation, inconsistent with simple laser-ablation induced mass-dependent fractionation. One or more other dominant ratio biasing processes are thus indicated.

Instrumental mass bias at the plasma-interface region cannot explain the effect. The constancy of the measured $^{205}Tl/^{203}Tl$ ratio displayed by Fig. 4D demonstrates that the concurrently variable Pb isotope ratios (Fig. 4C) are not due to fluctuations in mass bias at this region such as could be caused by variations in matrix composition during fluid inclusion ablation. Such matrix variations are likely to be subtle in any case, because the bulk aerosol load in the plasma is dominated by host quartz contribution, as the beam size is chosen to exceed the largest diameter of the fluid inclusion in order to ensure complete ablation[2,9].

The observed isotope ratio trends thus appear to be closely linked to problems associated with the recording of transient signals characterized by rapidly changing intensities. Evolving isotope ratios for transient analyte signals have been reported for thermal desorption of Hg from gold traps[40] and for analytes supplied by gas chromatography[41,42] or liquid chromatography[43]. Whereas such observations, at least in part, are likely to relate to real

mass fractionation effects accompanying the pre-processing of the analyte prior to its introduction to the plasma, bias can also be expected from the recording electronics of the instrument such as caused by differences in amplifier response among the Faraday collectors employed for multi-collector measurements. A quantitative treatment of this problem is presented in the following section.

Amplifier response bias: numerical correction schemes

Several studies involving transient signal processing have shown that isotopic ratios derived from rapidly rising or decreasing signals can be affected by amplifier response[12,43,19]. Such variations are also displayed by the $^{208}Pb/^{206}Pb$ isotope ratios of two fluid inclusions analyzed by the straight ablation technique (Fig. 5A) and by the stepwise opening procedure (Fig. 5D), respectively. Variations in $^{208}Pb/^{206}Pb$ correlate with intensity variation between sequential 0.2 s readings, which is particularly evident in the stepwise opened fluid inclusion (Fig. 5D). Variations in isotopic ratio during a static multiple collector measurement are therefore expected from any differences in the settling parameters of the Faraday amplifiers used in the analysis. Uncorrected, the amplifier outputs will lag behind the input (ion) signal after a change of beam intensity, and depending on which amplifiers are faster or slower, signals become enhanced or reduced relative to each other. Ratio bias is thus a function of input signal gradient and opposite for positive and negative gradients (Fig. 5D; see also Fig. 1 in Hirata et al.[12]).

Here, we present two approaches to correct for this problem, which we will call (1) the stepping *tau* correction and (2) the quadratic *tau* correction. In essence, signal decay functions are empirically determined for each Faraday detector and then applied to remove residual bias resulting from prior signal variations from the individual readings. To this aim, the existing instrument software of Nu Plasma 1700 was modified and expanded to allow for calibration of settling parameters required for each of the 16 Faraday amplifiers of the instrument. A typical calibration procedure consisted of repeat exposures of the Faraday collector to ion beams of ~ $8 * 10^{-11}$ A (using 10^{11} Ω feedback resistors) for 60 s, each followed by a measurement of the signal decay curve vs. time for another 60 s after beam cut-off. The timing chosen for such an experiment depend on the decay characteristics of the particular system to be calibrated. For adequate processing of fast transient signals, proper calibration of the decay segment extending over fractions of seconds to a few seconds immediately following beam cut-off is of great importance. This requires a fast mechanism for cutting the beam. Rather than relying on the standard method of applying a voltage offset to the electrostatic analyzer (ESA) for beam deflection, we use a pair of vertical deflectors located at the exit region of the ESA, which allows for faster beam control. The measurement of beam intensity and signal decay is performed at 0.1 s integration, the fastest reading rate available for the digital voltmeters (DVMs) used. Each DVM reading is associated with a time stamp read from the high-resolution performance counter of the computer controlling the instrument. A series of such measurements was bracketed between two baseline

measurements of 60 s each, preceded by waiting intervals of 180 s at beam-off conditions allowing the collector system to fully discharge. In order to derive amplifier response parameters, which then can be applied to correct the measurements, we model the decay curve as a sum of discrete RC decay terms

$$res(t) = \sum_{j=1}^{n} a_j \cdot e^{-t/\tau_j} \qquad (1)$$

where *res (t)* denotes the baseline-corrected residual signal intensity *t* seconds after beam cut-off divided by the baseline-corrected beam intensity, a_j is a pre-exponential coefficient, τ_j = R_jC_j the time constant for the j^{th} term, and *n* is the number of summation terms required to adequately reproduce the decay curve. $\sum_{j=1}^{n} a_j = 1$, such that *res(0)* = 1, equivalent to the full signal at the time of beam cut-off.

For proper application of this model to the real experiment, one needs to consider that the signal readings are based on integration over intervals of time rather than point measurements in time. To describe the decay curve as observed by integrated readings, equation 1 is rewritten as

$$resInt(t) = \sum_{j=1}^{n} \frac{a_j \cdot \tau_j}{\Delta t} \cdot \left(e^{-\frac{t}{\tau_j}} - e^{-\frac{t+\Delta t}{\tau_j}} \right) \qquad (2)$$

where *resInt(t)* is the residual signal as seen by integration over the time interval from *t* to *t* + Δt, *t* being the time elapsed since beam cut-off. From the repeat decay experiments, mean values and their errors are calculated for the signals and their time stamps, to serve as input data for the determination of the decay parameters a_j and τ_j by error weighted least-squares regression on equation 2. For the Faraday amplifiers of our instrument, $n \geq 4$ typically provides for adequate fitting of the decay curves over their recorded lengths.

A simple application of these parameters for correction of the measurements is to treat the intensity variation between subsequent readings as a step response function such that equation 2 can be applied to this task. For a series of readings sequentially integrated for Δt s each, the m^{th} reading, after correction based on the preceding *m-1* corrected readings, is

$$c_m = \left\{ m_m + \sum_{i=2}^{m-1} \left[(c_i - c_{i-1}) \cdot resInt(t_m - t_i) \right] - c_{m-1} \cdot resInt(0) \right\} \cdot \left[1 - resInt(0) \right]^{-1} \qquad (3)$$

where *c* refers to corrected readings, m_m is the measured reading currently to be corrected, and *resInt(...)* is defined by equation 2, with the values of the expressions in parentheses being substituted for *t*. For computational purposes the corrected readings together with their time stamps are stored in a rotating buffer of *m* elements, *m* depending on the time span over which an amplifier settling effect is resolvable in the data. We refer to this scheme as the *stepping tau correction*.

Equation (3) can be applied on- or off-line and results in adequate correction of ratio *trends* caused by amplifier response effects (Fig. 5B). However, it cannot easily cope with noisy or spiky signal behaviour, introducing excess variance to ratio data (Fig. 5E). To better treat such fast intensity variations, we apply a quadratic scheme referred to as *quadratic tau correction* to derive a continuous function for approximation of beam intensities within a given integration interval based on the measured data set. We begin by approximation of beam intensity *s* as a function of time *t* by a polynomial of second degree

$$s = h \cdot t^2 + k \cdot t + l\,, \tag{4}$$

which, for the i^{th} reading, s_i, becomes

$$sInt_i = h \cdot \left(t_i^{\,2} + t_i \cdot \Delta t + \frac{\Delta^2 t}{3} \right) + k \cdot \left(t_i + \frac{\Delta t}{2} \right) + l \tag{5}$$

when integrated from t_i to $t_i + \Delta t$ and divided by Δt , with t_i being the starting time of an integration interval of Δt duration. For each reading *i*, the coefficients *h*, *k* and *l* are determined by solving a system of three such equations using the measured *sInt* and *t* values at readings *i - 1, i*, and *i + 1*.

We will now use the signal variation given by equation (4) as a base for deriving a function which can be applied for *tau* correction of *sequential* readings. The signal bias caused by signal variation during an interval Δt at a time point located *t* seconds after the start and outside of this interval can be written as a sum of infinitesimal contributions from the signal variations during that interval, using the step response function implied by equation (1):

$$res(t) = \sum_{j=1}^{n} a_j \sum_{i=2}^{m} \left[h^* \cdot (i-1)^2 \cdot \Delta^2 x + k^* \cdot (i-1) \cdot \Delta x - h^* \cdot i^2 \cdot \Delta^2 x - k^* \cdot i \cdot \Delta x \right] \cdot e^{(i \cdot \Delta x - t)/\tau_j}$$

$$= \Delta x \cdot \sum_{j=1}^{n} a_j \sum_{i=2}^{m} \left[h^* \cdot \Delta x \cdot (1-2i) - k^* \right] \cdot e^{(i \cdot \Delta x - t)/\tau_j}\,. \tag{6}$$

a_j , τ_j and *n* are as defined for equation (1), h^* and k^* are similar to *h* and *k* used in equation (4), but calculated setting *t = 0* for the start of the interval. The variable *i* refers to the i^{th} infinitesimal signal step of Δx duration, with $\sum_{i=1}^{m} \Delta x = \Delta t$ corresponding to the duration of the actual integration interval. Note that equation (6) and the following equations are based on the real (unknown) beam intensities rather than on registered intensities modified by amplifier response. For $\Delta x \to 0$, equation (6) can be replaced by the sum of the integrals

$$res(t) = -\sum_{j=1}^{n} a_j \cdot \int_0^{\Delta t} \left(2 \cdot h^* \cdot x + k^* \right) \cdot e^{(x-t)/\tau_j} \cdot dx \quad , \tag{7}$$

which gives

$$res(t) = -\sum_{j=1}^{n} a_j \cdot \tau_j \cdot e^{-t/\tau_j} \cdot \left\{ \left[2 \cdot h^* \cdot (\Delta t - \tau_j) + k^* \right] \cdot e^{\Delta t/\tau_j} + 2 \cdot h^* \cdot \tau_j - k^* \right\}. \tag{8}$$

As for equation (2), equation (8) needs to be integrated to obtain the appropriate correction for a signal reading of Δt duration starting t seconds after the start of the interval responsible for the residual:

$$resInt(t) = \frac{1}{\Delta t} \cdot$$

$$\sum_{j=1}^{n} a_j \cdot {\tau_j}^2 \cdot e^{-t/\tau_j} \cdot \left\{ \left[2 \cdot h^* \cdot \left(\Delta t - \tau_j \right) + k^* \right] \cdot e^{\Delta t/\tau_j} + 2 \cdot h^* \cdot \tau_j - k^* \right\} \cdot \left(e^{-\Delta t/\tau_j} - 1 \right) \quad (9)$$

For equations (6) to (9) to be valid, $t \geq \Delta t$ is an essential condition, i.e., the integration interval to be corrected shall not overlap with the interval responsible for the residual. However, because beam variations within a given integration interval strongly affect the remaining part of the same interval, we need to derive a modified equation for this special case, using a similar approach, but observing variable integration boundaries. The result is

$$resInt(0) = \frac{1}{\Delta t} \cdot$$

$$\sum_{j=1}^{n} a_j \cdot \tau_j \cdot \left\{ \tau_j \cdot \left[2 \cdot h^* \cdot \left(\Delta t - \tau_j \right) + k^* + e^{-\Delta t/\tau_j} \cdot \left(2 \cdot h^* \cdot \tau_j - k^* \right) \right] - h^* \cdot \Delta^2 t - k^* \cdot \Delta t \right\} \quad (10)$$

To then correct a set of m continuous intensity readings s_i for amplifier response, we start at reading s_1 (assuming that this reading is not biased by earlier signal variation), determine h^* and k^* (using readings 1, 2 and 3 in this special case) and derive the correction value for reading 1 by equation (10). Equations (9) and (10) are then applied to derive corrections for reading 2 and so on, summing and storing the correction values derived from all previous signal readings (by equation (9)) and the internal correction (by equation (10)) separately for each reading. When the full data array has been processed, the correction values (residuals) are subtracted from their respective readings. As the signal shifts resulting from these corrections are not yet accounted for by the algorithm, the procedure is iterated, but rather than using the measured readings, the stored correction values from the previous pass are used for input. Iteration is stopped, when the correction values fall below a given threshold. In contrast to the step-function based correction algorithm given by equation (3), the current scheme can only be applied in off-line mode.

Figure 5 illustrates the improvement achieved with the two *tau* correction procedures. Uncorrected inclusion signals produced by straight ablation technique show pronounced ratio evolution coincident with the rising part of the signal, which is characterized by steep intensity gradient, while the slower signal decay during complete consumption of inclusion content has a much smaller effect (Fig. 5A). In contrast, the isotope ratios of the same inclusion corrected in stepping mode (Fig. 5B) shows fairly uniform isotope ratios that tend to become somewhat heavier with progressive ablation. The quadratic *tau* correction results in an even smoother trend (Fig. 5C), We interpret this residual trend to heavier values to relate to subordinate laser-ablation and aerosol transport induced isotope fractionation varying by *ca.* 0.5 % a.m.u.$^{-}$

[1]. This trend, however, does not affect the accuracy of the final isotope ratios, if the measurements are properly evaluated (see below).

Signals of inclusions ablated with the stepwise opening technique are characterized by abrupt decays and rises when the laser beam is blanketed off for increasing laser beam diameter and by fluctuations stemming from irregularities in the ablation rate of the inclusion (Fig. 5D). This results in considerable scatter of the raw ratios, which is only moderately reduced by *tau* correction in stepping mode (Fig. 5E). Although the use of the quadratic *tau* correction scheme further reduces these ratio excursions (Fig. 5F), there still remains variability in isotope ratios which negatively affects data precision. The residual bias could either be due to a non-ideal behavior of amplifiers or inaccurate tracking of the ion signals using relatively long (0.2 s) integration timing, or both, enhanced by the ultrafast changes in signal intensity related to the stop-and-go process associated with laser-beam size increase. We cannot exclude the possibility, however, that there is also some contribution by mass fractionation effects arising from generation and transport of the laser aerosol. Moreover, this particular fluid inclusion analysis showed some breakout during beam size increase at reading 56; hence, ablation was not well controlled.

The examples given in Fig.5 demonstrate that it is important to critically evaluate transient signal shapes during data reduction. Individual inclusions yield the best results if the transient signal is as smooth as possible, which is most likely achieved by straight ablation without deliberate interruptions for changing crater diameter. Robust data can thus be obtained on fluid inclusions, given that data evaluation is coupled with an appropriate *tau* correction.

Mass bias correction strategies

Two different within-run mass bias correction strategies based on Tl were explored, (a) Tl provided from within the inclusion and (b) desolvated Tl admixed to the laser ablation aerosol. This section focuses exclusively on results obtained by the individual reading data reduction method, to better illustrate differences.

In strategy (a) synthetic inclusions containing a mixture of SRM 981 Pb and SRM 997 Tl were measured while aspirating a 1% HNO_3 blank solution through the desolvation unit. Because such inclusions serve as common source for both Pb and Tl, it should, in principle, be possible to correct for the combined effects of mass fractionation generated during inclusion ablation, aerosol transport, ion production, and ion extraction in the source of the ICP-MS (i.e., instrumental mass bias sensu stricto), provided that Pb and Tl are affected in the same systematic fashion during fluid inclusion analysis and that the Pb-Tl fractionation parameters derived from SRM 610 glass ablation experiments are applicable to that process. The Pb-Tl fluid inclusion results listed in Table A2 demonstrate that the mean isotopic ratios of individual inclusions overlap at the 2 SD level with the nominal Pb isotope ratios of SRM 981[31], with uncertainties as low as 0.2 % 2 SD for $^{208}Pb/^{206}Pb$ and $^{207}Pb/^{206}Pb$ ratios, and *ca.* 0.4 % for Pb isotope ratios normalized to mass 204. This compares favourably with external

analytical precisions on fast transient signal measurement by MC-ICP-MS s reported by other studies (*e.g.,* for Hg: ≤4 ‰[40]). Scatter exceeding analytical error is apparent in some cases for data not corrected for amplifier response (*e.g.,* Pb-Tl fluid inclusions analyzed Aug30-05; Table A2) where individual Pb-Tl fluid inclusions were measured more precisely (down to 0.1 % for all Pb isotope ratios), returning significantly different isotope ratios for individual fluid inclusions that sometimes also deviate from the reference values (e.g., Pb-Tl_FI-5_Aug30-05). The distribution of Tl in the analyzed fluid inclusions is heterogeneous, as revealed by the Pb/Tl intensity ratios monitored during the analyses. Most inclusions showed some decoupling of the Tl signal structure from that of the Pb isotopes, possibly resulting from ablation of tiny Tl-enriched crystals existing in the inclusions or early release of Tl from the inclusion (Fig. 2A, B). The precision obtained, in particular for smaller inclusions, also suffers from low Tl signals which do not permit precise mass bias correction on a reading-to-reading basis.

For the smaller and flatter Pb-only inclusions, there is only a limited data set with adequate analytical precision for evaluation of strategy (b) (Table A2). Even for these inclusions, however, accurate results can be obtained by adding the Tl required for mass bias correction via desolvating nebulisation up-torch to the LA aerosol generated from Pb-only inclusions (Table 4, and below). Because of the low average intensities on mass 204 (2 - 6 x 10^{-14} A) obtained for these smaller inclusions, the $^{20X}Pb/^{204}Pb$ ratios measured on individual inclusions are less precise than those measured for the larger Pb-Tl inclusions.

In order to further test the applicability of the Tl admixture approach, an assemblage of 20-30 µm sized Pb-Tl inclusions (n=12) was analyzed by addition of Tl from the desolvating unit, exactly as done for the Pb-only inclusions. These data (Table 4) reveal an overall better inclusion-to-inclusion reproducibility for $^{208}Pb/^{206}Pb$ and $^{207}Pb/^{206}Pb$ ratios at within-run precisions even better than those obtained for larger Pb-Tl inclusions when analyzed without Tl admixture (this also holds for the Pb-Tl fluid inclusion data collected during the same session on Aug 30; Table A2). This supports our view that inclusion-to-inclusion analytical reproducibility can suffer from limitations on mass bias correction imposed by low-intensity fluid inclusion Tl signals and by non-uniform distribution of Tl in our synthetic Pb-Tl fluid inclusions. Most importantly, however, our tests demonstrate that accurate data can be obtained for the Pb isotope analysis of an individual fluid inclusion and that these tests do not resolve any disadvantage in admixing desolvated Tl to the laser ablation aerosol for mass bias correction.

Individual reading versus entire signal integration

To further investigate ablation trends and to better define a strategy for choosing interval limits for fast transient signal analysis, the isotope ratios calculated for individual 0.2 s integration intervals from a set of inclusions with Tl admixed from a desolvator (Table 4) were averaged over four types of signal intervals (Fig. 6A), (1) first part of the signal covering the signal rise from the baseline to the peak, (2) second part of the signal, from the peak down to

572 the baseline, (3) a “wide” interval, comprising both the first and the second parts of the signal,
573 and (4) a “widest best-precision” interval which selects the segment optimizing the internal
574 precision of the $^{208}Pb/^{206}Pb$ and $^{207}Pb/^{206}Pb$ ratios while maintaining the integration interval as
575 large as possible. The results plotted in Fig. 6B demonstrate that $^{208}Pb/^{206}Pb$ in the first part of
576 the ablation at rising signal intensity is generally significantly heavier, while the second half of
577 the signal at dropping signal intensity the ratio tends to be lighter than the averages
578 calculated for the “wide” and the “widest best-precision” intervals. The latter most closely
579 approximate the true value. This pattern becomes considerably modified for *tau*-corrected
580 data (bottom graph), with a slight predominance of light Pb during the first part of the signal
581 trace and heavier Pb during the second part (as observed for an individual inclusion analysis;
582 Figs. 5B, C). The ratios with ^{204}Pb in the denominator are not shown, because they are not
583 precise enough to reveal the trends.

584 The given examples demonstrate that one needs to integrate the entire transient signal,
585 which can be done in essentially two ways, named here the *individual reading integration*
586 method and the *bulk signal integration* method. Using the individual reading integration
587 method, each reading is weighed equally for deriving the final isotopic ratio of the sample.
588 This approach may be inadequate for the analysis of highly transient signals, where signal
589 intensities may vary by more than two orders of magnitude during sample analysis, because
590 low-intensity readings yield ratios of poorer precision compared to high-intensity readings.
591 Cutting off the low-intensity wings of the transient signals altogether is also not desirable,
592 because such portions of the ablation signal are often highly fractionated and their omission
593 can bias the final result (compare Figs. 5 and 6).

594 Intensity-weighted average isotope ratios of transient signals are expected to be more
595 representative, because low-intensity and possibly highly fractionated and/or imprecise
596 readings exert less weight in averaging. This is partially equivalent to *bulk signal integration*,
597 i.e., to the summation of signal intensities over a chosen signal section (*e.g.,* Evans et al.[40])
598 before applying the data reduction scheme to these integrated signal values. A drawback of
599 this scheme is that information about isotope ratio evolution across the transient signal as
600 addressed above is lost and that no information on internal errors can directly be gained from
601 the data. Minimum estimates for the uncertainty of isotope ratios as calculated by the bulk
602 signal integration method can, however, be obtained from Gaussian combination of ion
603 statistics and baseline noise. Adopting an average value of 3.2×10^{-16} A (1 SD of baseline
604 readings integrated for 1 s) for the latter, we have generated estimates for the uncertainties
605 listed in Table 4 using Monte Carlo techniques. Note that these uncertainties do not include
606 systematic and random errors associated with *tau* correction.

607 Figure 7 compares three data sets of the same 20 fluid inclusion analyses reduced by the
608 individual reading integration method (i) and the bulk signal integration method (ii, iii), each
609 applied to the same number of readings per fluid inclusion. (i) and (ii) use data not corrected
610 for amplifier response, while for (iii) they were corrected using the stepping *tau* correction

scheme. The most prominent difference is the increase in accuracy when using the bulk signal integration method, even without *tau* correction (compare (i) and (ii) in Fig. 7A). In addition, the two outliers in the $^{208}Pb/^{206}Pb$ ratio resulting from poorly controlled fluid inclusion ablation can no longer be deemed outliers when using the bulk signal integration method with *tau* correction; hence, the effect of poorly controlled fluid inclusion ablation may in part be mitigated by use of the summed signal intensities of the entire signal interval. The same improvement is not observed for ratios normalized to mass 204 (Fig. 7B), due to limited measurement precision on mass 204.

The best accuracy (Fig. 7) for a fast transient signal analysis is obtained by the bulk signal integration method (see also Cottle et al.[19]). Given the limitations in transient data recording that, to our knowledge, apply to all currently used MC-ICP-MS instruments to variable degree, our findings conform to the notion that successful methods of transient signal analysis rely on integration schemes that use most of the transient signal, i.e., essentially the entire sample, for isotope ratio determination. For fluid inclusions specifically, this requires controlled ablation by the straight ablation technique and recording of the entire inclusion content. Fluid inclusions vary in size (thus in total amount of Pb available for analysis) and geometries (translating to different transient signal shapes); hence, the quality of individual fluid inclusion analyses varies significantly. The laser ablation and aerosol transport processes together with the commonly sub-ng amounts of Pb available for analysis likely dominate the overall analytical uncertainty of an individual fluid inclusion for *tau* corrected signal recordings. Therefore, the Pb isotope composition of the fluid is best represented by the uncertainty-weighted average isotopic composition calculated from a series of individually analyzed fluid inclusions that belong to a fluid inclusion assemblage (see Pettke[9] for more information).

An example of natural fluid inclusions

Data obtained on samples of fluid inclusions from porphyry-type ore deposits demonstrate that the analytical precision obtained on natural samples can be even better than that documented above for our fluid inclusion standards (Table 5). Figure 8 illustrates the data obtained on the Nu Plasma instrument. The reproducibility obtained for two inclusion assemblages (*i.e.*, coevally entrapped individual inclusions on a single healed microfracture in quartz, representing individual samples of an isotopically uniform fluid[9]) from one vein quartz sample serves as a good example for the data quality achievable for fluid inclusion Pb isotope analysis. Here, the inclusion-to-inclusion reproducibility is *ca.* 0.05 % (2 SD; n=11) for $^{208}Pb/^{206}Pb$ and $^{207}Pb/^{206}Pb$, and *ca.* 0.13% for Pb isotope ratios with mass 204 in the denominator (data calculated by bulk signal integration). The uncertainties expressed as two standard errors of the mean of the 11 inclusion analyses are *ca.* 0.016 and *ca.* 0.04 %, respectively.

Based on our results obtained on synthetic fluid inclusions, these analyses are considered to be accurate within their calculated precisions. Potential interferences in chemically complex natural fluid inclusions may include chloride ions of rare earth elements (REE; lanthanide group) or polyatomic argide ions. Concentrations of middle to heavy REE are low in normal crustal fluids, and the analysis of the SRM 610 glass containing approximately 440 μg g^{-1} each of REE did not reveal such problems. The synthetic fluid inclusion standards are well suited for evaluating the production of metal-hydride ions or peak tailing effects, and such problems have not been identified in the current data set. In some geological environments, Hg may represent a significant component, in which case the measured $^{202}Hg/^{200}Hg$ ratio can be used to characterize mass bias for interference correction at mass 204. Mercury interference correction on mass 204 based on the Tl proxy as used in this study is considered robust for fluid inclusions when Hg is a rare component (i.e., $^{202}Hg/^{204}Pb < 0.1$). Isobaric interference by WO^+ ions on ^{202}Hg, on the other hand, could potentially result in an inappropriate Hg interference correction but, typically, W concentrations in fluid inclusions are rather low except for hot magmatic-hydrothermal fluids originating from highly fractionated silicate melts associated with Sn-W ore deposits (*e.g.,* Audétat et al.[44]). In such a case, ^{201}Hg could be used for mass bias correction instead, unless interfered by ReO^+, which is unlikely to be present in significant concentrations in high-salinity brine inclusions. ^{201}Hg may thus be an alternative choice for Hg interference correction for specific natural samples. It is thus concluded that accurate data can be obtained from the analysis of individual natural fluid inclusions even for complex solution compositions (*e.g.*, Pettke et al.[21]).

Concluding remarks

The MC-ICP-MS analytical procedures for Pb isotope ratios recorded in transient data acquisition mode are developed here for fast transient signals as produced by laser ablation of individual fluid inclusions. Extensive testing demonstrates:

- Differences in amplifier response among Faraday detectors are often not adequately accounted for by commercial instruments. We thus present rigorous *tau* correction schemes and demonstrate their success.
- To obtain accurate isotope ratios, transient signals need to be integrated and processed as an entity.
- Signals integrated using the individual reading method on *tau*-corrected data reveal that Pb isotope ratios become heavier with progressive fluid inclusion ablation, which we ascribe to laser-ablation induced isotope fractionation. The magnitude of this fractionation is small and not relevant for the analyses of individual fluid inclusions presented here.

- Results for an individual fluid inclusion are best calculated using the bulk signal integration method, whereby high-intensity readings have correspondingly greater weight in defining the overall isotope ratios.
- Mass bias correction based on Tl admixed as desolvated aerosol to the laser ablation aerosol can generate highly accurate data.
- Individual fluid inclusions are best analyzed by the straight ablation technique; stepwise opening causes fast changes in signal intensities requiring larger and less-precise corrections for amplifier response.
- Interferences typically pose no limitations to data accuracy in our application to saline and Pb-rich (0.1 wt % Pb) magmatic-hydrothermal fluid inclusions.

The external precision achieved on MC-ICP-MS instruments for repetitive analysis of SRM 610 glass is shown to converge to ± 0.011 % (2 SD) for $^{208}Pb/^{206}Pb$ and $^{207}Pb/^{206}Pb$ ratios and to ± 0.032 % (2 SD) for Pb isotope ratios measured relative to mass 204, or 0.0026 and 0.0075 % 2SE (n=18), respectively, significantly more precise than LA-ICP-MS results obtained on single collector instruments as reported in the literature. The challenge of analyzing an individual fluid inclusion lies in the fact that it contains a strictly limited mass of analyte, of the order of 0.1 ng of Pb for an inclusions 40x40x30 µm in size, to be measured during a short time interval. External reproducibilities obtained on natural fluid inclusion assemblages were as good as *ca.* 0.05 % 2 SD (n=11) for $^{208}Pb/^{206}Pb$ and $^{207}Pb/^{206}Pb$, and *ca.* 0.13% for Pb isotope ratios normalized to mass 204. Acceptably reproducible results (± 0.1 % and 0.5 %, respectively) were obtained for inclusions containing as little as 0.005 ng Pb with the current procedure.

Our study shows that a standard LA-MC-ICP-MS instrument equipped with Faraday detectors such as Nu Plasma or Nu Plasma 1700 can successfully be employed for Pb isotope analysis of individual fluid inclusions. MC-ICP-MS instruments equipped with multiple ion counters can significantly reduce the amount of Pb required for analysis, but accuracy has been shown to be somewhat limited (to *ca.* ±0.1 % uncertainty) due to ion counter gain stability issues[13,45]. This is about an order of magnitude higher than the analytical precision obtained here for $^{208}Pb/^{206}Pb$ and $^{207}Pb/^{206}Pb$ ratios on SRM 610 glass. Ion counting, however, would be of advantage for the analysis of low-Pb samples provided that careful data acquisition schemes (*e.g.,* Cottle et al.[19]) are combined with the rigorous signal integration procedure introduced here.

Acknowledgments

TP and CAH acknowledge financial support from the Swiss National Science Foundation (grants Nr. PP002-106569 and 200020-107955). We also would like to thank E. Rosu for field assistance in Romania, and the technical staff at IGP, ETH Zurich, for their continued excellent support for analytical instrumentation. Heinrich Baur and Donat Niederer have been

particularly helpful in the investigation of Faraday amplifier technical issues. We thank the 2 reviewers for pointing out the issues that needed clarification.

References

1 P. Sylvester, *Mineral. Assoc. Can. Short Course Series,* 2008, **40**, pp. 348.

2 D. Günther, A. Audétat, R. Frischknecht and C. A. Heinrich, *J. Anal. At. Spectrom.,* 1998, **13**(4), 263-270.

3 A. Audétat, D. Günther and C. A. Heinrich, *Science*, 1998, **279**, 2091-2094.

4 W. E. Halter, T. Pettke, C. A. Heinrich and B. Rothen-Rutishauser, *Chem. Geol.,* 2002, **183**, 63-86.

5 C. A. Heinrich, T. Pettke, W. E. Halter, M. Aigner-Torres, A. Audétat, D. Günther, B. Hattendorf, D. Bleiner, M. Guillong and I. Horn, *Geochim. Cosmochim. Acta,*2003, **67**, 3473-3497.

6 T. Pettke, W. E. Halter, J. D. Webster, M. Aigner-Torres, and C. A. Heinrich, *Lithos,* 2004, **78**, 333-361.

7 M. M. Allan, B. W. D. Yardley, L. J. Forbes, K. I. Shmulovich, D. A. Banks and T. J. Shepherd, *Am. Mineral.,* 2005, **90**, 1767-1775.

8 C. Spandler, J. Mavrogenes and J. Hermann, *Chem. Geol.,* 2007, **239**, 228-249.

9 T. Pettke, *Mineral. Assoc. Can. Short Course Series,* 2008, **40**, 189-218.

10 A. J. Walder, I. D. Abell, I. Platzner and P. A. Freedman, *Spectrochim. Acta B-Atom. Spectrosc.,* 1993, **48**, 397-402.

11 T. Hirata, *J. Anal. At. Spectrom.,* 2002, **17**, 204-210.

12 T. Hirata, Y. Hayano and T. Ohno,*J. Anal. At. Spectrom.,* 2003, **18**, 1283-1288.

13 B. Paul, J. D. Woodhead and J. Hergt, *J. Anal. At. Spectrom.,* 2005, **20**(12), 1350-1357.

14 J. Kosler, R. B. Pedersen, C. Kruber and P. J. Sylvester, *J. Anal. At. Spectrom.,* 2005, **20**, 192-199.

15 M. G. Jackson and S. R. Hart, *Earth Planet. Sci. Lett.,* 2006, **245**, 260-277.

16 C. Paton, J. D. Woodhead, J. M. Hergt, D. Phillips and S. Shee, *Geostand. Geoanalyt. Res.,* 2007, **31**, 321-330

17 M. Gounelle, E. D. Young, A. Shahar, E. Tonui and A Kearsley, *Earth Planet. Sci. Lett.,* 2007, **256**, 521-533.

18 J. Fietzke, V. Liebetrau, D. Günther, K. Gürs, K. Hametner., K. Zumholz, T. H. Hansteen and A. Eisenhauer, *J. Anal. At. Spectrom.,* 2008, **23**, 955-961.

19 J. M. Cottle, M. S. A. Horstwood and R. R. Parrish, *J. Anal. At. Spectrom.,* 2009, **24**, 1355-1363.

20 J. Woodhead, J. Hergt, S. Meffre, R. R. Large, L. Danyushevsky and S. Gilbert, *Chem. Geol.,* 2009, **262**, 344-354.

21 T. Pettke, F. Oberli and C. A. Heinrich, *Earth Planet. Sci. Lett.*, 2010, **296**, 267-277.

22 M. Rehkämper and K. Mezger, *J. Anal. At. Spectrom.,* 2000, **15**, 1451-1460.

23 J. Woodhead, *J. Anal. At. Spectrom.,* 2002, **17**, 1381-1385.

24 M. F. Thirlwall, *Chem. Geol.,* 2002, **184**, 255-279.

25 F. Albarède, P. Telouk, J. Blichert-Toft, M. Boyet, A. Agranier and B. Nelson, *Geochim. Cosmochim. Acta,* 2004, **68**, 2725-2744.

26 D. C. Baxter, I. Rodushkin, E. Engstrom and D. Malinovsky, *J. Anal. At. Spectrom.,* 2006 , **21**, 427-430.

27 S. E. Jackson and D. Günther, *J. Anal. At. Spectrom.,* 2003, **18**, 205-212.

28 B. Kuhn, K. Birbaum, Y. Luo, and D. Günther, *J. Anal. At. Spectrom.,* 2010, **25**, 21-27.

29 A. N. Halliday, D. C. Lee, J. N. Christensen, M. Rehkämper, W. Yi, X. Z. Luo, C. M. Hall , C. J. Ballentine, T. Pettke and C. Stirling, *Geochim. Cosmochim. Acta,*1998, **62**, 919-940.

30 H. P. Longerich, B. J. Fryer and D. F. Strong, *Spectrochim. Acta B-Atom. Spectrosc.,* 1987, **42**, 39-48.

31 J. Baker, D. Peate, T. Waight and C. Meyzen, *Chem. Geol.,* 2004, **211**, 275-303.

32 A. Audétat, D. Günther and C. A. Heinrich, *Econ. Geol.*, 2000b, **95**, 1563-1581.

33 T. Pettke, U. H. Wiechert, A. Audétat, D. Günther and C. A. Heinrich, *Geochim. Cosmochim. Acta,* 2003, **67**, A378.

34 T. Pettke T., C. A. Heinrich, A. C. Ciocan, and D. Günther, *J. Anal. At. Spectrom.,* 2000, **15**, 1149-1155.

35 G. D., Kamenov, P. A. Mueller and M. R. Perfit, *J. Anal. At. Spectrom.,* 2004, **19**, 1262-1267.

36 L. P. Dunstan, J. W. Gramlich, I. L. Barnes and W. C. Purdy, *J. Res. Nat. Bureau Stand.,* 1980, **85**, 1-10.

37 S. M. Eggins and J. M. G. Shelley, *Geostand. Newslett.,* 2002, **26**(3), 269-286.

38 A. J.R. Kent, *Geostand. Geoanalyt. Res.,* 2008a, **32**, 129-147.

39 B. J. A. Willigers, J. A. Baker, E. J. Krogstad and D. W. Peate, *Geochim. Cosmochim. Acta,*2002, **66**, 1051-1066.

40 R. D. Evans, H. Hintelmann, and P. J. Dillon, *J. Anal. At. Spectrom.,* 2001, **16**, 1064-1069.

41 S. Wehmeier, R. Ellam and J. Feldmann, *J. Anal. At. Spectrom.,* 2003, **18**, 1001-1007.

42 E. A. Krupp and O. F. X. Donard, *Intl. J. Mass Spec.,* 2005, **242**, 233-242.

43 I. Günther-Leopold, J. Kobler Waldis, B. Wernli and Z. Kopajtic, *Int. J. Mass Spectrom*. 2005, **242**, 197-202.

44 A. Audétat, D. Günther and C. A. Heinrich, *Geochim. Cosmochim. Acta*, 2000a, **64**, 3373-3393.

45 A. K. Souders and P. J. Sylvester, *J. Anal. At. Spectrom.,* 2008, **23**, 535-543.

46 A. J.R. Kent, *J. Anal. At. Spectrom.,* 2008b, **23**, 968-975.

Figure captions

Fig. 1. Synthetic fluid inclusion standards containing SRM 981 Pb + SRM 997 Tl (A) or SRM 981 Pb only (B) in a Na-K-Cl solution of *ca.* 17 wt% bulk salinity. Note the ellipsoidal to isometric shape of the Pb-Tl fluid inclusions, while the Pb-only fluid inclusions are generally flat, irregular and smaller.

Fig. 2. Pb and Tl transient isotope signals from fluid inclusion ablation recorded on multiple Faraday detectors. (A, C) Straight ablation (at constant crater size), (B) step-wise fluid inclusion opening. Signals from large Pb-Tl inclusions (A, B) are characterized by Pb/Tl ratios evolving with progressive inclusion ablation, with signal maxima for Tl shifted towards the start of the ablation. (C) Pb-only inclusion signal produced from inclusion ablation and recorded together with the Tl signal originating from aspirating a SRM 997 Tl solution through a desolvating unit. LA stands for laser ablation.

Fig. 3. (A) $^{207}Pb/^{204}Pb$ vs. $^{208}Pb/^{206}Pb$ laser ablation data of SRM 610 glass show that correction for mass-dependent isotope fractionation (mass bias) following Baxter et al.[26] leaves no residual correlation. (B) A plot of isotope ratios with mass 204 in the denominator reveals a linear trend, indicative of correlation due to elevated uncertainty for mass 204. Error bars are 2SE measurement uncertainties.

Fig. 4. Plot of background-corrected Pb (A, C) and Tl (B, D) isotope ratios (filled circles) calculated for individual 0.2 s integration intervals (readings), and corresponding total Pb and Tl signal intensities (open squares). The sections shown cover the entire signal interval integrated for two fluid inclusion analyses. Both fluid inclusions were liberated by the straight ablation technique. All the isotope ratios are plotted at the same scale. Trend lines (dotted) are shown in A, B and C. Raw Pb isotopic ratios evolve for both Pb-Tl inclusions (A) and Pb-only inclusions (C). For Pb-Tl inclusions, the measured $^{205}Tl/^{203}Tl$ ratio (all Tl supplied by the inclusion) also evolves with progressive ablation of the inclusion (B), while it remains constant for the Pb-only inclusions (D), where Tl is supplied from desolvated aerosol. Note the larger scatter of isotope ratios at the beginning and end of the transient signal trace (A, B), resulting from reduced analytical precision at the low-intensity tails. The evolution of the background-corrected Pb isotopic ratios during progressive fluid inclusion ablation is mainly due to differences in response of the Faraday amplifiers used for recording the masses (see Fig. 5 and text for explanations).

Fig. 5. Plots of background-corrected Pb isotope ratios calculated for individual 0.2 s integration readings for two fluid inclusions measured by the straight ablation (A-C) and the stepwise opening (D-F) technique, uncorrected and corrected for amplifier response as indicated and detailed in text. Measured total Pb intensities are given by the grey curves. Note that the isotope ratios (black dots) are plotted at the same scale. Dashed lines drawn at $^{208}Pb/^{206}Pb = 2.22$ in A-C are given for visual reference

only. $^{208}Pb/^{206}Pb$ ratios not corrected for amplifier response show up to 10 % scatter that is reduced through correction to *ca.* 1%.

Fig. 6. Lead isotope ratios from 20 fluid inclusions integrated across different segments of the transient signals using the individual reading integration method. Internal mass bias correction is based on Tl admixed from a desolvator. (A) is an example of intervals chosen for integration; “First” refers to first part of the signal trace, “Second” to the second part, wide encompasses both the first and second part of the signal, and the “Widest best precision” is calculated as explained in the text. (B) shows Pb isotope data without correction for amplifier response. Substantially elevated $^{208}Pb/^{206}Pb$ ratios are observed for the first part of the signal, while the second part is generally lighter than both the “wide” and the “widest best-precision” signal averages, which overlap for a given inclusion ablation. (C) shows the same data corrected for amplifier response as detailed in the text. Although considerably reduced in magnitude, there remains a systematic offset between the averages the first and second half of the fluid inclusion signals for several inclusion analyses, interpreted to relate to isotope fractionation at the laser ablation site (compare Figs. 5B, C). Error bars are 95% C.I. following Baxter et al.[26].

Fig. 7. External reproducibility plots for $^{208}Pb/^{206}Pb$ (A) and $^{207}Pb/^{204}Pb$ (B) ratios for 20 individual fluid inclusion (20-25 µm diameter) analyses using aspirated Tl for mass bias correction. Greyed data points were discarded from the averaged data set, due to uncontrolled fluid inclusion ablation, which may generate precise measurements of unconstrained accuracy. Thick grey lines represent nominal values for SRM 981[31]. Black dots (i) represent data obtained by the individual reading integration method using the widest best precision interval (data set A in Table 4) with 2 SE measurement uncertainties. Open (ii) and filled (iii) black squares represent isotope ratios calculated by the bulk signal integration method, with a lower limit of uncertainty estimated from a Gaussian combination of ion statistics and baseline noise. Filled black squares (iii) are calculated using data corrected for amplifier response (data set B in Table 4), while open squares (ii) represent uncorrected data. Data obtained by the bulk signal integration method (ii and iii) are significantly more accurate and scatter less for isotope ratios normalized to ^{206}Pb while its effect is not so obvious for isotope ratios normalized to ^{204}Pb, due to the low precision of the ^{204}Pb measurements. See text for explanation.

Fig. 8. $^{207}Pb/^{206}Pb$ (A) and $^{207}Pb/^{204}Pb$ (B) isotope ratios determined for 12 fluid inclusions of *ca.* 40x30x30 µm size from a natural vein quartz sample analyzed with desolvated Tl aerosol admixed for mass bias correction. Inclusions from assemblages A and B show indistinguishable Pb isotopic compositions. The greyed data point identifies an outlier. Error bars are 2 SE measurement uncertainties.

Table 1:
Measured Pb and Tl concentrations, and nominal salinity of synthetic fluid inclusion standards

Sample	NaCl wt-% nominal	KCl wt-% nominal	Pb µg g^{-1} analyzed	Tl µg g^{-1} analyzed
Pb-C1	11.7	6.2	5700	—
Pb-C3	11.7	6.2	5070	—
Pb-C5	11.7	6.2	5480	—
Pb-Tl-A2	10.5	5.9	4030	1510
Pb-Tl-A3	10.5	5.9	4430	1640

No data available for synthesis Pb-Tl-A4
The nominal Pb concentration in runs Pb-C1 to Pb-C5 was 5500 µg per g of fluid,
that in Pb-Tl-A2 and Pb-Tl-A3 was 5200 µg g^{-1}
The nominal Tl concentration in runs Pb-Tl-A2 and A3 was1790 µg per g of fluid,
— Absent from synthesis

Table 2:
LA-ICP-MS instrument and data acquisition parameters

Compex 110I Excimer 193 nm ArF laser

- Energy density on sample (J/cm^2)	Ca. 16 (10 - 25), homogeneous energy distribution across the ablation crater
- Pulse duration (ns)	Ca. 15
- Repetition rate (Hz)	SRM: 6 (1 - 10), FI: 10
- Shooting mode	1 µm s^{-1} line scan (SRM), single spot (SRM, FI)
- Crater sizes (µm)	SRM: 60, variable for FI (8 - 80)
- Ablation cell volume (cm^3)	FI: 1, variable for SRM (1 - 16)
- Helium cell gas flow (l min^{-1})	0.5 - 0.8 (0.3 - 1.3)

Nu Plasma MC-ICP-MS

- Desolvating nebulizer unit	MCN-6000
- Process gas	Ar
- Power (W)	1400 (1100 - 1500) fwd.; <2 refl.
- Accelerating voltage (kV)	4
- Detector mode	Multiple Faradays
- Mass resolution	ca. 400 (10 % valley)

Nu Plasma 1700 MC-ICP-MS

- Desolvating nebulizer unit	DSN-100 (Nu Instruments Ltd)
- Process gas	Ar
- Power (W)	1450 (1100 - 1550) fwd.; <2 ref.
- Accelerating voltage (kV)	6
- Detector mode	Multiple Faradays
- Mass resolution per a.m.u.	ca. 700 (10 % valley)

Data acquisition parameters during transient signal analysis, both instruments

- Acquisition mode	Static
- Integration time	200 ms per reading
- Baseline measurement	On peak with laser beam off
- Masses analyzed	200, 202, 203, 204, 205, 206, 207, 208

Notes:
Values reported in brackets are the ranges explored
SRM refers to SRM 610 glass from NIST
FI refers to fluid inclusions

Table 3: Selected LA-ICP-MS data for SRM 610 glass bracketing fluid inclusion analyses

Run	$^{208}Pb/^{206}Pb$ final	1 SE abs	$^{207}Pb/^{206}Pb$ final	1 SE abs	$^{206}Pb/^{204}Pb$ final	1 SE abs	$^{207}Pb/^{204}Pb$ final	1 SE abs	$^{208}Pb/^{204}Pb$ final	1 SE abs
NU Plasma 1700: August 30										
SRM610_Aug30-05_1	2.16932	0.00015	0.90988	0.00004	17.0502	0.0017	15.5136	0.0018	36.9836	0.0050
SRM610_Aug30-05_2	2.16919	0.00014	0.90987	0.00004	17.0505	0.0018	15.5139	0.0019	36.9851	0.0052
SRM610_Aug30-05_3	2.16908	0.00016	0.90978	0.00004	17.0484	0.0020	15.5098	0.0022	36.9782	0.0060
SRM610_Aug30-05_4	2.16910	0.00015	0.90978	0.00004	17.0457	0.0017	15.5071	0.0018	36.9697	0.0052
SRM610_Aug30-05_5	2.16920	0.00014	0.90977	0.00004	17.0515	0.0018	15.5117	0.0019	36.9853	0.0053
SRM610_Aug30-05_6	2.16912	0.00015	0.90976	0.00004	17.0484	0.0017	15.5105	0.0019	36.9789	0.0053
SRM610_Aug30-05_7	2.16935	0.00013	0.90986	0.00003	17.0522	0.0018	15.5142	0.0017	36.9889	0.0046
SRM610_Aug30-05_8	2.16905	0.00014	0.90982	0.00004	17.0492	0.0018	15.5109	0.0019	36.9776	0.0052
SRM610_Aug30-05_9	2.16923	0.00013	0.90980	0.00003	17.0474	0.0016	15.5096	0.0017	36.9778	0.0045
SRM610_Aug30-05_10	2.16921	0.00016	0.90982	0.00004	17.0461	0.0021	15.5088	0.0021	36.9715	0.0058
SRM610_Aug30-05_11	2.16933	0.00015	0.90989	0.00004	17.0483	0.0021	15.5118	0.0021	36.9799	0.0058
SRM610_Aug30-05_12	2.16924	0.00015	0.90982	0.00004	17.0488	0.0020	15.5109	0.0019	36.9779	0.0052
SRM610_Aug30-05_13	2.16922	0.00013	0.90983	0.00003	17.0456	0.0017	15.5082	0.0017	36.9720	0.0047
SRM610_Aug30-05_14	2.16937	0.00014	0.90991	0.00004	17.0463	0.0017	15.5100	0.0017	36.9743	0.0046
SRM610_Aug30-05_15	2.16928	0.00013	0.90987	0.00003	17.0471	0.0017	15.5106	0.0017	36.9759	0.0048
SRM610_Aug30-05_16	2.16953	0.00012	0.90992	0.00003	17.0449	0.0017	15.5107	0.0018	36.9790	0.0048
SRM610_Aug30-05_17	2.16910	0.00013	0.90980	0.00004	17.0443	0.0018	15.5065	0.0019	36.9655	0.0051
SRM610_Aug30-05_18	2.16942	0.00012	0.90984	0.00003	17.0415	0.0019	15.5056	0.0019	36.9692	0.0051
daily average	2.16924		0.90984		17.0476		15.5102		36.9772	
2 SD (absolute)	0.00026		0.00010		0.0054		0.0048		0.0123	
2 SD (ppm)	119		105		318		310		334	
2 SE (absolute)	0.00006		0.00002		0.00128		0.00113		0.00291	
2 SE (ppm)	28		25		75		73		79	
NU Plasma: August 23										
SRM610_1	2.16988	0.00017	0.90996	0.00004	17.0562	0.0035	15.5186	0.0031	37.0057	0.0073
SRM610_2	2.17000	0.00022	0.91003	0.00006	17.0620	0.0041	15.5270	0.0037	37.0223	0.0088
SRM610_20	2.17007	0.00021	0.91001	0.00005	17.0628	0.0050	15.5266	0.0047	37.0230	0.0110
SRM610_21	2.16976	0.00015	0.90995	0.00004	17.0475	0.0030	15.5131	0.0028	36.9884	0.0070
SRM610_22	2.16981	0.00015	0.90994	0.00004	17.0437	0.0031	15.5098	0.0028	36.9846	0.0070
SRM610_23	2.16991	0.00014	0.90996	0.00004	17.0417	0.0027	15.5092	0.0026	36.9792	0.0066
SRM610_24	2.16952	0.00015	0.90992	0.00004	17.0524	0.0029	15.5173	0.0027	36.9948	0.0068
SRM610_30	2.16997	0.00015	0.90998	0.00004	17.0451	0.0031	15.5126	0.0030	36.9867	0.0074
SRM610_31	2.17003	0.00015	0.91003	0.00004	17.0450	0.0031	15.5112	0.0029	36.9868	0.0071
SRM610_32	2.17014	0.00014	0.91008	0.00004	17.0482	0.0028	15.5153	0.0026	36.9961	0.0065
SRM610_33	2.16976	0.00015	0.90996	0.00005	17.0463	0.0032	15.5125	0.0029	36.9869	0.0072
daily average	2.16990		0.90998		17.0501		15.5157		36.9959	
2 SD (absolute)	0.00035		0.00009		0.0146		0.0124		0.0299	
2 SD (ppm)	162		104		856		797		809	
2 SE (absolute)	0.00011		0.00003		0.0044		0.0037		0.0090	
2 SE (ppm)	49		31		258		240		244	

Notes: All shots were acquired in line scan mode (1 µm s^{-1} transport rate, 6Hz, 60 µm spot size)
Uncertainties given for individual fluid inclusions are 1 standard error of measurement

Table 4: LA-ICP-MS Pb isotope results of individual synthetic fluid inclusions analysed in session August 30, 2005, on Nu Plasma 1700

	FI chip number	FI size (µm)	Ablation quality †	$^{208}Pb/^{206}Pb$ final	Error abs ‡	# of readings	$^{207}Pb/^{206}Pb$ final	Error abs ‡	# of readings	$^{206}Pb/^{204}Pb$ final	Error abs ‡	# of readings	$^{207}Pb/^{204}Pb$ final	Error abs ‡	# of readings	$^{208}Pb/^{204}Pb$ final	Error abs ‡	# of readings
SRM 981 reference values (Baker et al.[4])				2.1678			0.9149			16.94			15.50			36.73		
(A) August 30, 2005: Results obtained by the individual time slice integration method, not corrected for amplifier response																		
Pb_FI-1_Aug30-05	C1	35	+++	2.1645	0.0023	47 of 50	0.9138	0.0008	47 of 50	16.98	0.06	46 of 50	15.54	0.05	47 of 50	36.82	0.13	48 of 50
Pb_FI-2_Aug30-05	*C1*	*35*	*exploded*	*2.1610*	0.0042	*36 of 39*	*0.9124*	0.0013	*37 of 39*	*17.05*	0.09	*37 of 39*	*15.57*	0.09	*37 of 39*	*36.90*	0.23	*37 of 39*
Pb_FI-3_Aug30-05	*C1*	*35*	*exploded*	*2.1609*	0.0028	*38 of 40*	*0.9130*	0.0007	*38 of 40*	*16.96*	0.02	*39 of 40*	*15.50*	0.02	*37 of 40*	*36.67*	0.07	*39 of 40*
Pb_FI-4_Aug30-05	C1	30	+++	2.1644	0.0020	69 of 74	0.9138	0.0007	70 of 74	16.90	0.09	69 of 74	15.46	0.09	70 of 74	36.65	0.21	69 of 74
Pb_FI-5_Aug30-05	C1	60	+++	2.1664	0.0010	127 of 135	0.9143	0.0004	128 of 135	16.98	0.05	129 of 135	15.53	0.05	129 of 135	36.83	0.11	128 of 135
Pb_FI-6_Aug30-05	C3	30	+++	2.1673	0.0021	85 of 87	0.9146	0.0006	83 of 87	16.99	0.07	81 of 87	15.55	0.06	80 of 87	36.85	0.16	82 of 87
Pb_FI-7_Aug30-05	C3	70	+++	2.1681	0.0009	194 of 204	0.9147	0.0004	194 of 204	16.98	0.05	191 of 204	15.54	0.04	192 of 204	36.83	0.10	191 of 204
Pb_FI-8_Aug30-05	C3	30	+++	2.1665	0.0023	70 of 75	0.9142	0.0006	70 of 75	16.86	0.12	68 of 75	15.45	0.11	70 of 75	36.55	0.27	70 of 75
Pb-Tl_FI-9_Aug30-05	A4	30	++(+)	2.1657	0.0021	70 of 73	0.9140	0.0007	71 of 73	16.91	0.06	69 of 73	15.47	0.05	70 of 73	36.66	0.13	70 of 73
Pb-Tl_FI-10_Aug30-05	A4	35	+++	2.1676	0.0013	202 of 215	0.9146	0.0006	202 of 215	16.95	0.07	202 of 215	15.51	0.06	201 of 215	36.79	0.15	203 of 215
Pb-Tl_FI-11_Aug30-05	A4	25	++	2.1657	0.0018	93 of 99	0.9145	0.0007	93 of 99	16.95	0.10	94 of 99	15.51	0.09	92 of 99	36.69	0.19	92 of 99
Pb-Tl_FI-12_Aug30-05	A4	40	+++	2.1677	0.0017	113 of 117	0.9140	0.0007	110 of 117	17.00	0.06	108 of 117	15.53	0.06	109 of 117	36.83	0.14	109 of 117
Pb-Tl_FI-13_Aug30-05	A4	25	+++	2.1691	0.0014	97 of 103	0.9152	0.0005	98 of 103	16.96	0.06	97 of 103	15.53	0.05	96 of 103	36.81	0.12	96 of 103
Pb-Tl_FI-14_Aug30-05	A4	35	+++	2.1671	0.0019	74 of 78	0.9146	0.0005	75 of 78	16.90	0.07	72 of 78	15.46	0.06	73 of 78	36.60	0.15	73 of 78
Pb-Tl_FI-15_Aug30-05	A4	45	+++	2.1664	0.0023	66 of 68	0.9146	0.0007	65 of 68	16.99	0.07	62 of 68	15.53	0.06	61 of 68	36.81	0.15	61 of 68
Pb-Tl_FI-16_Aug30-05	A4	22	+++	2.1676	0.0019	89 of 91	0.9149	0.0006	87 of 91	17.03	0.07	83 of 91	15.59	0.06	82 of 91	36.92	0.14	81 of 91
Pb-Tl_FI-17_Aug30-05	A4	25	+++	2.1691	0.0018	92 of 98	0.9151	0.0006	92 of 98	16.91	0.11	92 of 98	15.46	0.10	91 of 98	36.65	0.23	91 of 98
Pb-Tl_FI-18_Aug30-05	A4	50	++(+)	2.1667	0.0021	80 of 86	0.9146	0.0008	79 of 86	16.99	0.14	82 of 86	15.54	0.13	82 of 86	36.83	0.31	82 of 86
Pb-Tl_FI-19_Aug30-05	A4	30	+++	2.1686	0.0014	114 of 116	0.9155	0.0005	109 of 116	16.93	0.08	108 of 116	15.51	0.07	108 of 116	36.74	0.18	109 of 116
Pb-Tl_FI-20_Aug30-05	A4	30	+++	2.1675	0.0019	76 of 80	0.9147	0.0007	75 of 80	16.89	0.07	74 of 80	15.45	0.07	74 of 80	36.62	0.17	74 of 80
Average				2.1670			0.9145			16.95			15.51			36.75		
2 SD (absolute)				0.0027			0.0010			0.09			0.08			0.21		
2 SD (ppm)				1252			1048			5495			5442			5817		
2 SE (abs)				0.0006			0.0002			0.02			0.02			0.05		
2 SE (ppm)				295			247			1295			1283			1371		
(B) August 30, 2005: Results obtained by the bulk signal integration method, corrected for amplifier response																		
Pb_FI-1_Aug30-05	C1	35	+++	2.1678	0.0011	—	0.9145	0.0005	—	16.99	0.07	—	15.54	0.06	—	36.84	0.15	—
Pb_FI-2_Aug30-05	C1	35	exploded	2.1661	0.0016	—	0.9134	0.0008	—	17.04	0.14	—	15.57	0.13	—	36.91	0.30	—
Pb_FI-3_Aug30-05	C1	35	exploded	2.1678	0.0008	—	0.9146	0.0003	—	16.95	0.02	—	15.50	0.02	—	36.74	0.04	—
Pb_FI-4_Aug30-05	C1	30	+++	2.1656	0.0013	—	0.9137	0.0006	—	16.95	0.10	—	15.49	0.09	—	36.72	0.21	—
Pb_FI-5_Aug30-05	C1	60	+++	2.1679	0.0009	—	0.9145	0.0004	—	16.97	0.05	—	15.52	0.05	—	36.78	0.12	—
Pb_FI-6_Aug30-05	C3	30	+++	2.1676	0.0011	—	0.9146	0.0005	—	16.96	0.07	—	15.51	0.07	—	36.76	0.16	—
Pb_FI-7_Aug30-05	C3	70	+++	2.1683	0.0009	—	0.9148	0.0004	—	16.97	0.06	—	15.53	0.06	—	36.81	0.13	—
Pb_FI-8_Aug30-05	C3	30	+++	2.1672	0.0013	—	0.9143	0.0006	—	16.89	0.10	—	15.45	0.09	—	36.61	0.22	—
Pb-Tl_FI-9_Aug30-05	A4	30	++(+)	2.1687	0.0010	—	0.9147	0.0005	—	16.92	0.06	—	15.48	0.06	—	36.70	0.14	—
Pb-Tl_FI-10_Aug30-05	A4	35	+++	2.1684	0.0010	—	0.9148	0.0005	—	16.93	0.09	—	15.49	0.08	—	36.72	0.19	—
Pb-Tl_FI-11_Aug30-05	A4	25	++	2.1675	0.0013	—	0.9146	0.0006	—	16.96	0.10	—	15.51	0.09	—	36.76	0.21	—
Pb-Tl_FI-12_Aug30-05	A4	40	+++	2.1680	0.0010	—	0.9145	0.0005	—	16.99	0.08	—	15.54	0.07	—	36.83	0.16	—
Pb-Tl_FI-13_Aug30-05	A4	25	+++	2.1691	0.0009	—	0.9150	0.0004	—	16.97	0.05	—	15.53	0.05	—	36.81	0.12	—
Pb-Tl_FI-14_Aug30-05	A4	35	+++	2.1683	0.0011	—	0.9149	0.0005	—	16.93	0.07	—	15.49	0.07	—	36.72	0.15	—
Pb-Tl_FI-15_Aug30-05	A4	45	+++	2.1687	0.0010	—	0.9149	0.0005	—	17.00	0.06	—	15.55	0.06	—	36.87	0.13	—
Pb-Tl_FI-16_Aug30-05	A4	22	+++	2.1681	0.0011	—	0.9149	0.0005	—	17.00	0.08	—	15.55	0.07	—	36.85	0.17	—
Pb-Tl_FI-17_Aug30-05	A4	25	+++	2.1695	0.0013	—	0.9151	0.0007	—	16.93	0.10	—	15.49	0.10	—	36.72	0.22	—
Pb-Tl_FI-18_Aug30-05	A4	50	++(+)	2.1676	0.0017	—	0.9147	0.0009	—	16.98	0.16	—	15.53	0.15	—	36.81	0.34	—
Pb-Tl_FI-19_Aug30-05	A4	30	+++	2.1685	0.0011	—	0.9152	0.0005	—	16.95	0.08	—	15.51	0.07	—	36.75	0.17	—
Pb-Tl_FI-20_Aug30-05	A4	30	+++	2.1684	0.0011	—	0.9147	0.0006	—	16.88	0.09	—	15.44	0.08	—	36.61	0.20	—
Average				2.1681			0.9147			16.95			15.51			36.76		
2 SD (absolute)				0.0017			0.0007			0.07			0.06			0.15		
2 SD (ppm)				766			761			4004			4110			4028		
2 SE (abs)				0.0004			0.0002			0.02			0.02			0.03		
2 SE (ppm)				181			179			944			969			949		

Notes:

Values in italics were excluded from calculation of averages because fluid inclusion ablation was not well ocntrolled

† Quality of fluid inclusion ablation as visually judged on monitor screen (+++ = excellent; ++ = acdeptable; + = poor)

‡ Refers to absolute uncertainties expressed for dataset A as 2 SE measurement errors, for dataset B as the 95% confidence limit calculated following Baxter et al. [26]

Table 5: Data for two natural fluid inclusion assemblages from the porphyry copper deposit at Rosia Poieni

Sample	FI size (µm)	Ablation quality †	208Pb/206Pb	CI 95% ‡	207Pb/206Pb	CI 95% ‡	206Pb/204Pb	CI 95% ‡	207Pb/204Pb	CI 95% ‡	208Pb/204Pb	CI 95% ‡
Individual reading integration; widest best precision interval												
050706_RP_FI-1	30	+++	2.05768	0.00111	0.83576	0.00070	18.648	0.027	15.603	0.020	38.369	0.054
050706_RP_FI-2	30	+++	2.05884	0.00114	0.83647	0.00105	18.644	0.026	15.603	0.016	38.379	0.047
050706_RP_FI-3	35	+++	2.05884	0.00087	0.83634	0.00047	18.649	0.019	15.601	0.017	38.390	0.042
050706_RP_FI-4	40	+++	2.05874	0.00100	0.83597	0.00048	18.655	0.017	15.603	0.016	38.414	0.043
050706_RP_FI-5	40	+++	2.05936	0.00116	0.83671	0.00071	18.644	0.040	15.603	0.033	38.396	0.088
050706_RP_FI-6	30	+++	2.05949	0.00101	0.83640	0.00073	18.657	0.021	15.609	0.016	38.414	0.049
050706_RP_FI-7	50	++(+)	2.05998	0.00107	0.83687	0.00077	18.671	0.021	15.621	0.016	38.461	0.049
050706_RP_FI-8	*75*	++	*2.05841*	*0.00068*	*0.83585*	*0.00033*	*18.674*	*0.012*	*15.615*	*0.009*	*38.442*	*0.025*
050706_RP_FI-9	35	+++	2.05912	0.00115	0.83653	0.00105	18.635	0.021	15.596	0.013	38.367	0.041
050706_RP_FI-10	40	+++	2.06027	0.00103	0.83694	0.00095	18.674	0.021	15.625	0.013	38.472	0.042
050706_RP_FI-11	35	+++	2.05849	0.00079	0.83630	0.00038	18.641	0.020	15.593	0.015	38.363	0.043
050706_RP_FI-12	35	++(+)	2.05917	0.00119	0.83626	0.00081	18.631	0.029	15.589	0.020	38.349	0.057
average			**2.05909**		**0.83641**		**18.650**		**15.604**		**38.397**	
2 stdev (abs)			**0.00141**		**0.00071**		**0.027**		**0.022**		**0.080**	
2 stdev (ppm)			**686**		**848**		**1466**		**1391**		**2072**	
2 SE (abs)			**0.00043**		**0.00021**		**0.008**		**0.007**		**0.024**	
2 SE (ppm)			**207**		**256**		**442**		**419**		**625**	
Bulk signal integration; widest best precision interval												
050706_RP_FI-1	30	+++	2.05857	0.00088	0.83667	0.00029	18.650	0.018	15.604	0.016	38.391	0.042
050706_RP_FI-2	30	+++	2.05890	0.00089	0.83670	0.00029	18.644	0.016	15.600	0.014	38.386	0.040
050706_RP_FI-3	35	+++	2.05908	0.00083	0.83669	0.00028	18.649	0.016	15.603	0.015	38.398	0.039
050706_RP_FI-4	40	+++	2.05927	0.00091	0.83665	0.00028	18.658	0.014	15.610	0.013	38.421	0.038
050706_RP_FI-5	40	+++	2.05900	0.00098	0.83687	0.00031	18.641	0.022	15.600	0.019	38.381	0.051
050706_RP_FI-6	30	+++	2.05988	0.00089	0.83696	0.00028	18.648	0.014	15.608	0.013	38.413	0.037
050706_RP_FI-7	50	++(+)	2.06038	0.00089	0.83708	0.00028	18.665	0.013	15.625	0.012	38.457	0.036
050706_RP_FI-8	*75*	++	*2.05859*	*0.00072*	*0.83621*	*0.00025*	*18.668*	*0.010*	*15.611*	*0.009*	*38.429*	*0.025*
050706_RP_FI-9	35	+++	2.05939	0.00085	0.83689	0.00027	18.640	0.012	15.599	0.011	38.385	0.033
050706_RP_FI-10	40	+++	2.06034	0.00083	0.83701	0.00027	18.663	0.012	15.622	0.011	38.452	0.032
050706_RP_FI-11	35	+++	2.05861	0.00080	0.83673	0.00027	18.635	0.014	15.593	0.012	38.362	0.033
050706_RP_FI-12	35	++(+)	2.05935	0.00097	0.83697	0.00031	18.635	0.019	15.597	0.017	38.375	0.047
average			**2.05934**		**0.83684**		**18.648**		**15.606**		**38.402**	
2 stdev (abs)			**0.00124**		**0.00031**		**0.021**		**0.020**		**0.061**	
2 stdev (ppm)			**604**		**370**		**1124**		**1274**		**1596**	
2 SE (abs)			**0.00037**		**0.00009**		**0.006**		**0.006**		**0.018**	
2 SE (ppm)			**182**		**112**		**339**		**384**		**481**	
Bulk signal integration; wide interval												
050706_RP_FI-1	30	+++	2.05823	0.00074	0.83652	0.00027	18.650	0.020	15.601	0.017	38.385	0.043
050706_RP_FI-2	30	+++	2.05898	0.00080	0.83662	0.00027	18.651	0.017	15.604	0.014	38.401	0.038
050706_RP_FI-3	35	+++	2.05881	0.00076	0.83650	0.00027	18.656	0.017	15.606	0.015	38.408	0.039
050706_RP_FI-4	40	+++	2.05905	0.00079	0.83670	0.00027	18.647	0.015	15.602	0.013	38.394	0.035
050706_RP_FI-5	40	+++	2.05921	0.00081	0.83696	0.00029	18.641	0.024	15.602	0.021	38.385	0.052
050706_RP_FI-6	30	+++	2.06034	0.00079	0.83705	0.00027	18.660	0.014	15.619	0.013	38.444	0.034
050706_RP_FI-7	50	++(+)	2.05988	0.00076	0.83695	0.00026	18.665	0.013	15.622	0.012	38.447	0.032
050706_RP_FI-8	*75*	++	*2.05853*	*0.00064*	*0.83626*	*0.00024*	*18.669*	*0.009*	*15.612*	*0.008*	*38.429*	*0.021*
050706_RP_FI-9	35	+++	2.05992	0.00072	0.83693	0.00025	18.653	0.012	15.611	0.010	38.422	0.028
050706_RP_FI-10	40	+++	2.06026	0.00070	0.83698	0.00025	18.669	0.012	15.626	0.010	38.463	0.027
050706_RP_FI-11	35	+++	2.05870	0.00067	0.83671	0.00025	18.639	0.016	15.595	0.013	38.371	0.034
050706_RP_FI-12	35	++(+)	2.05908	0.00083	0.83672	0.00029	18.643	0.019	15.599	0.017	38.387	0.044
average			**2.05931**		**0.83679**		**18.652**		**15.608**		**38.410**	
2 stdev (abs)			**0.00137**		**0.00039**		**0.020**		**0.020**		**0.061**	
2 stdev (ppm)			**665**		**464**		**1051**		**1302**		**1580**	
2 SE (abs)			**0.00041**		**0.00012**		**0.006**		**0.006**		**0.018**	
2 SE (ppm)			**201**		**140**		**317**		**392**		**476**	

Notes: Values in italics were excluded from calculation of averages because fluid inclusion ablation was not well ocntrolled

† Quality of fluid inclusion ablation as visually judged on monitor screen (+++ = excellent; ++ = acceptable; + = poor)

‡ Refers to absolute uncertainties expressed as the 95% confidence limit calculated following Baxter et al.[26]

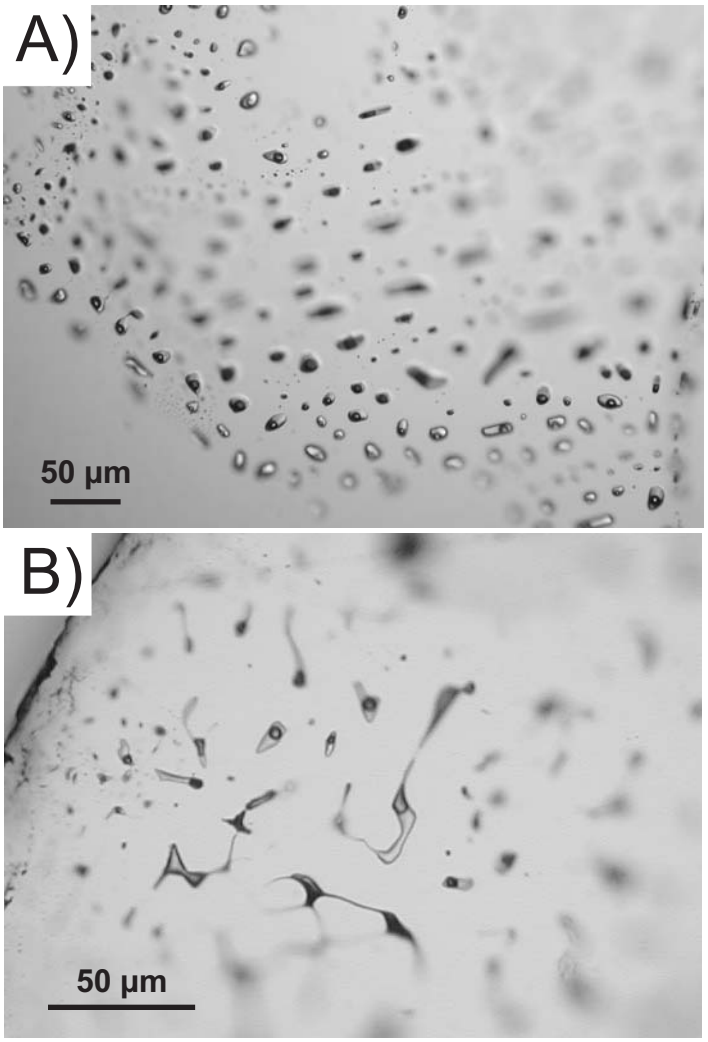

Figure 1

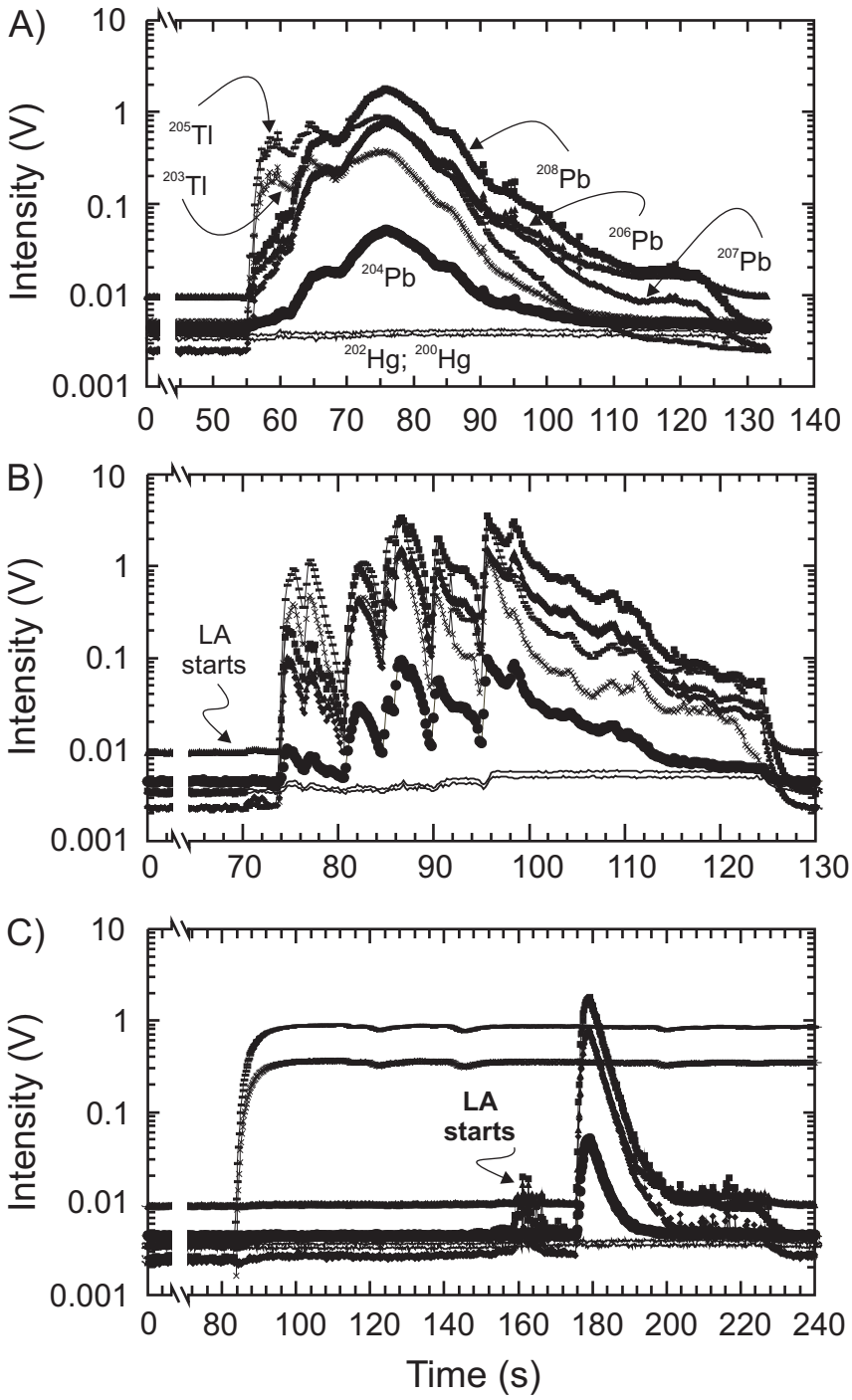
A)
B)
C)
Intensity (V)
10
1
0.1
0.01
0.001
^{205}Tl
^{203}Tl
^{208}Pb
^{206}Pb
^{207}Pb
^{204}Pb
^{202}Hg; ^{200}Hg
0 50 60 70 80 90 100 110 120 130 140
LA starts
0 70 80 90 100 110 120 130
LA starts
0 80 100 120 140 160 180 200 220 240
Time (s)

Figure 2

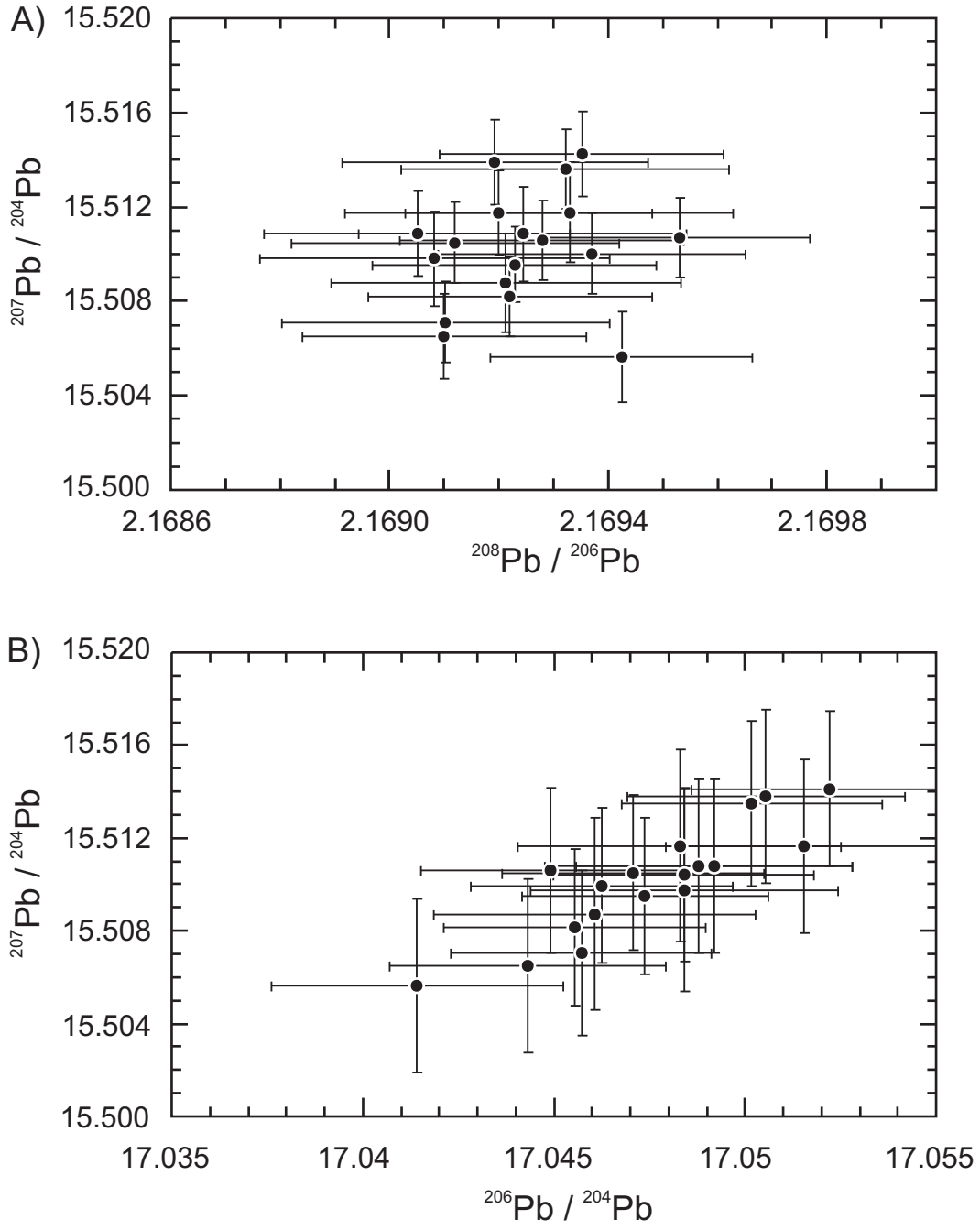
A)
15.520
15.516
15.512
15.508
15.504
15.500
^{207}Pb / ^{204}Pb
2.1686
2.1690
2.1694
2.1698
^{208}Pb / ^{206}Pb
B)
15.520
15.516
15.512
15.508
15.504
15.500
^{207}Pb / ^{204}Pb
17.035
17.04
17.045
17.05
17.055
^{206}Pb / ^{204}Pb

Figure 3

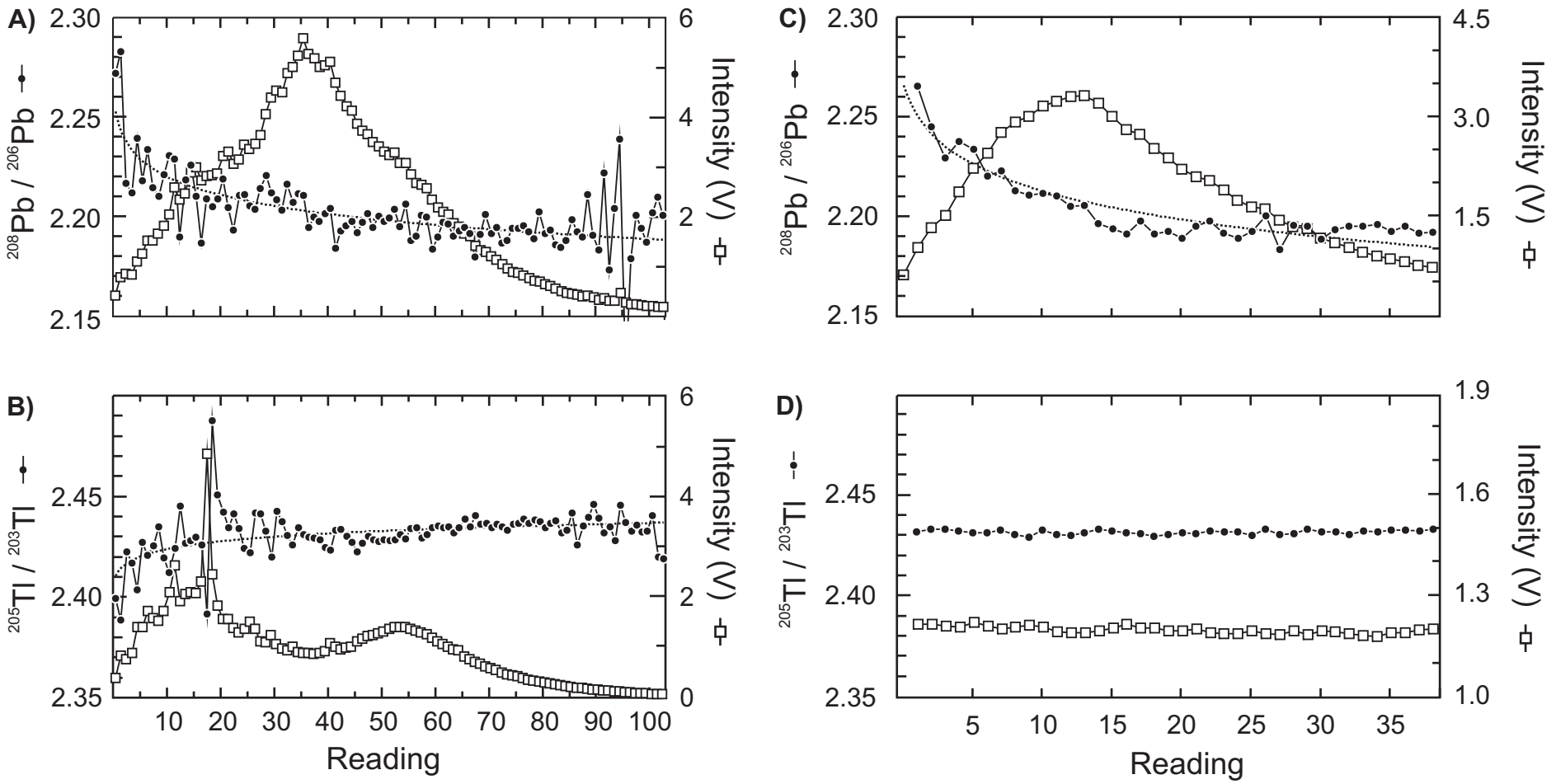

Figure 4

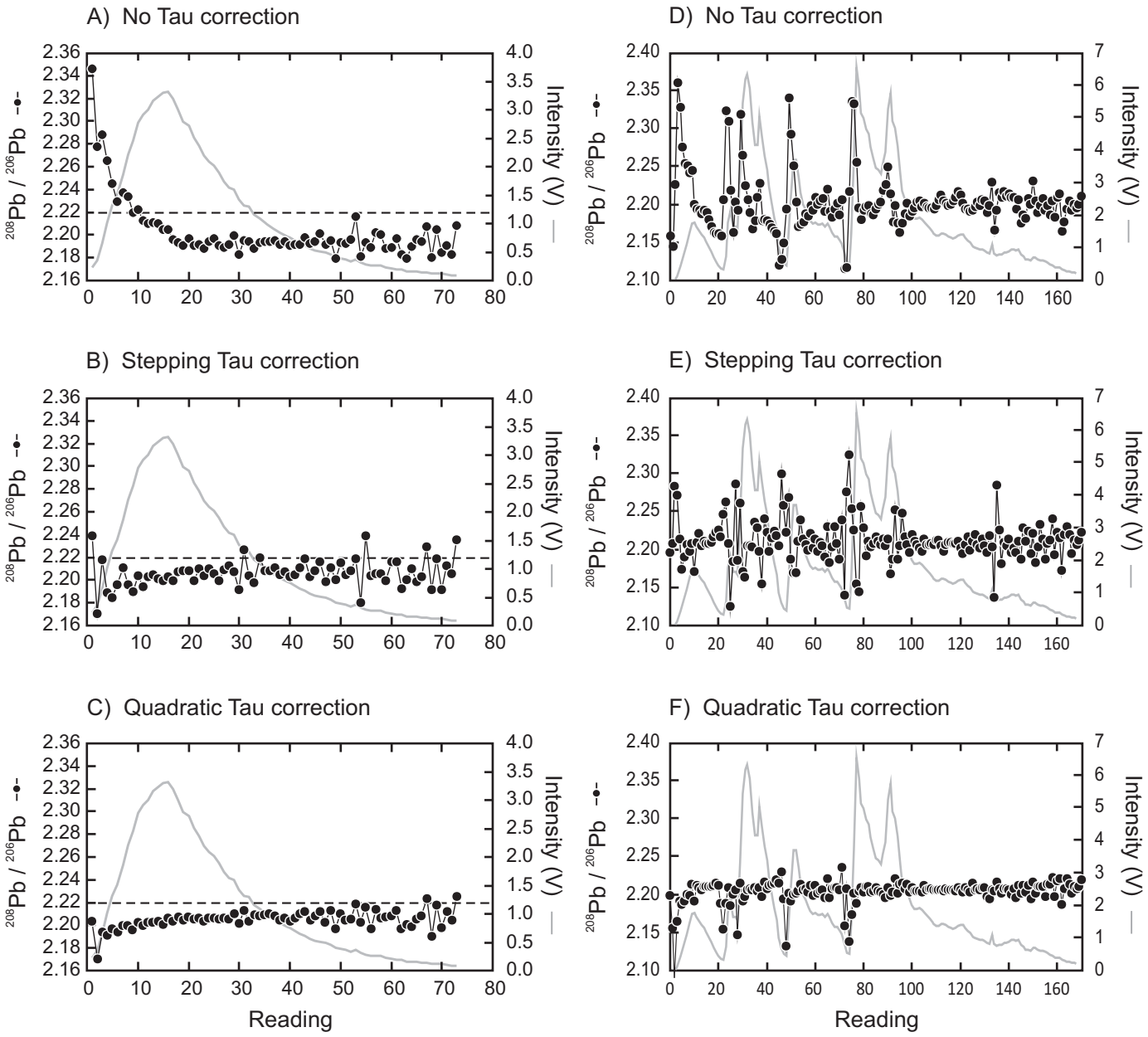
A) No Tau correction
B) Stepping Tau correction
C) Quadratic Tau correction
D) No Tau correction
E) Stepping Tau correction
F) Quadratic Tau correction
208Pb / 206Pb
Intensity (V)
Reading

Figure 5

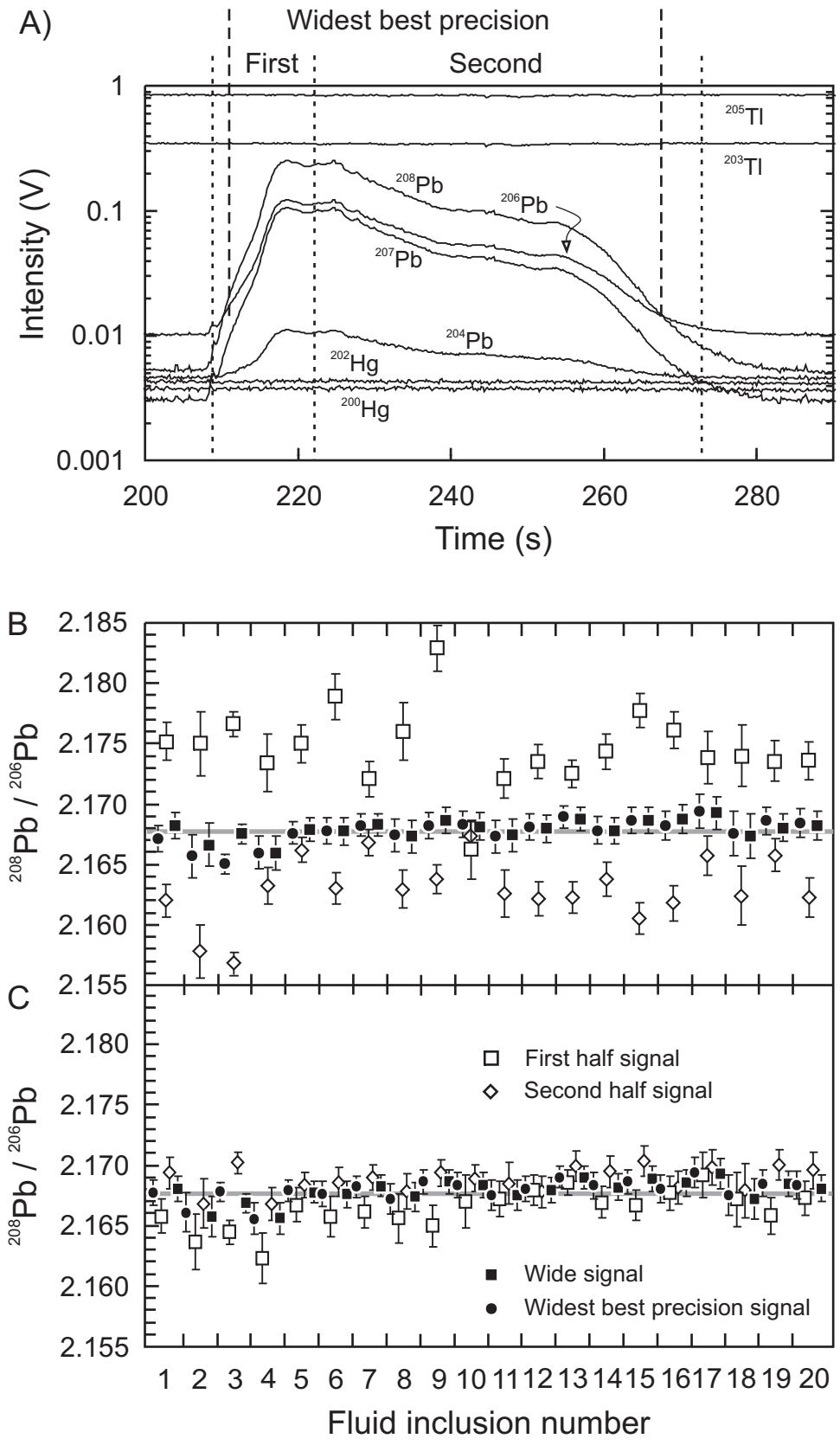
A)
Widest best precision
First
Second
Intensity (V)
1
0.1
0.01
0.001
205Tl
203Tl
208Pb
206Pb
207Pb
204Pb
202Hg
200Hg
200
220
240
260
280
Time (s)
B
C
208Pb / 206Pb
2.185
2.180
2.175
2.170
2.165
2.160
2.155
First half signal
Second half signal
Wide signal
Widest best precision signal
1 2 3 4 5 6 7 8 9 10 11 12 13 14 15 16 17 18 19 20
Fluid inclusion number

Figure 6

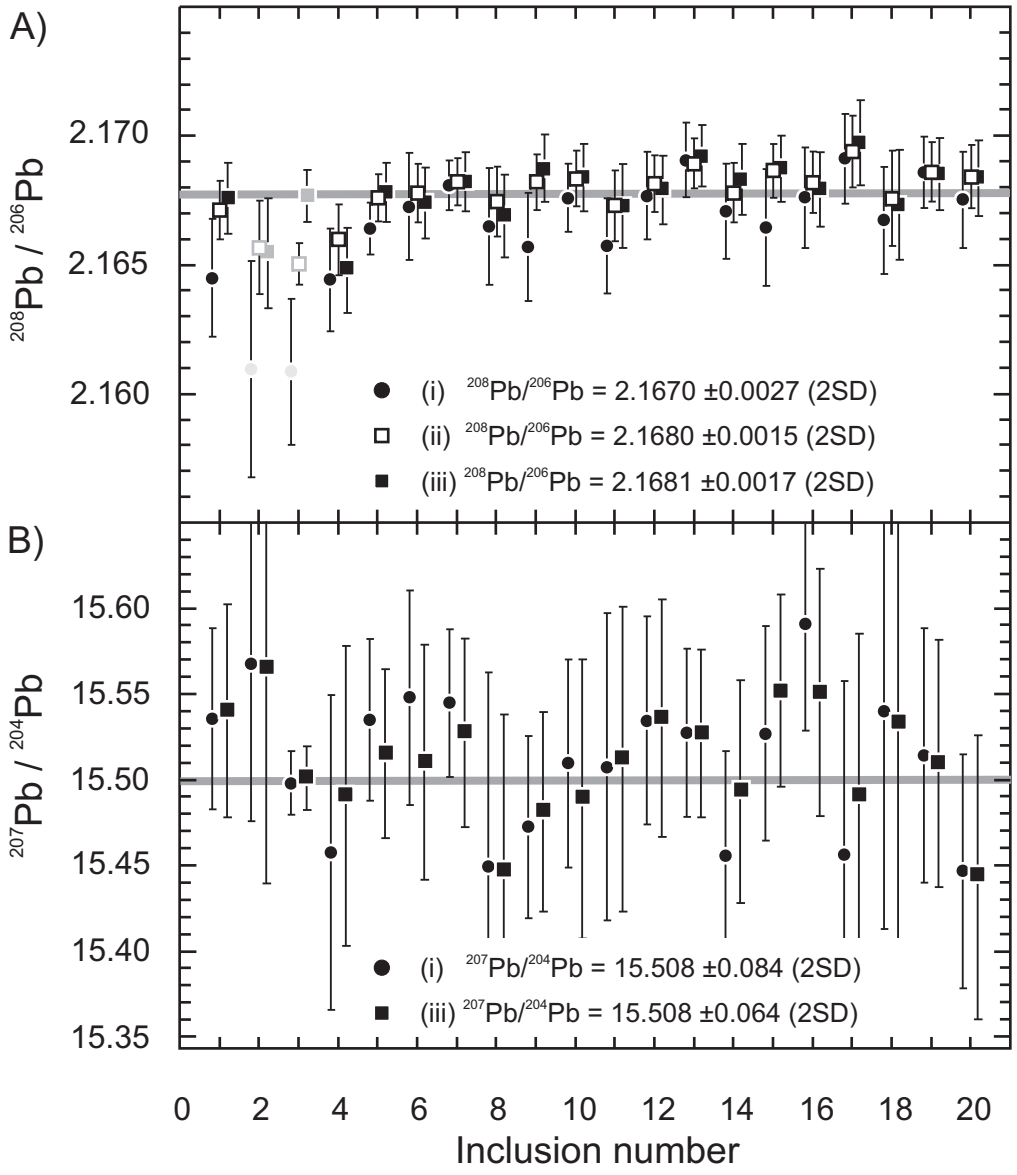
A)
^{208}Pb / ^{206}Pb
2.170
2.165
2.160
(i) $^{208}Pb/^{206}Pb$ = 2.1670 ±0.0027 (2SD)
(ii) $^{208}Pb/^{206}Pb$ = 2.1680 ±0.0015 (2SD)
(iii) $^{208}Pb/^{206}Pb$ = 2.1681 ±0.0017 (2SD)
B)
^{207}Pb / ^{204}Pb
15.60
15.55
15.50
15.45
15.40
15.35
(i) $^{207}Pb/^{204}Pb$ = 15.508 ±0.084 (2SD)
(iii) $^{207}Pb/^{204}Pb$ = 15.508 ±0.064 (2SD)
0
2
4
6
8
10
12
14
16
18
20
Inclusion number

Figure 7

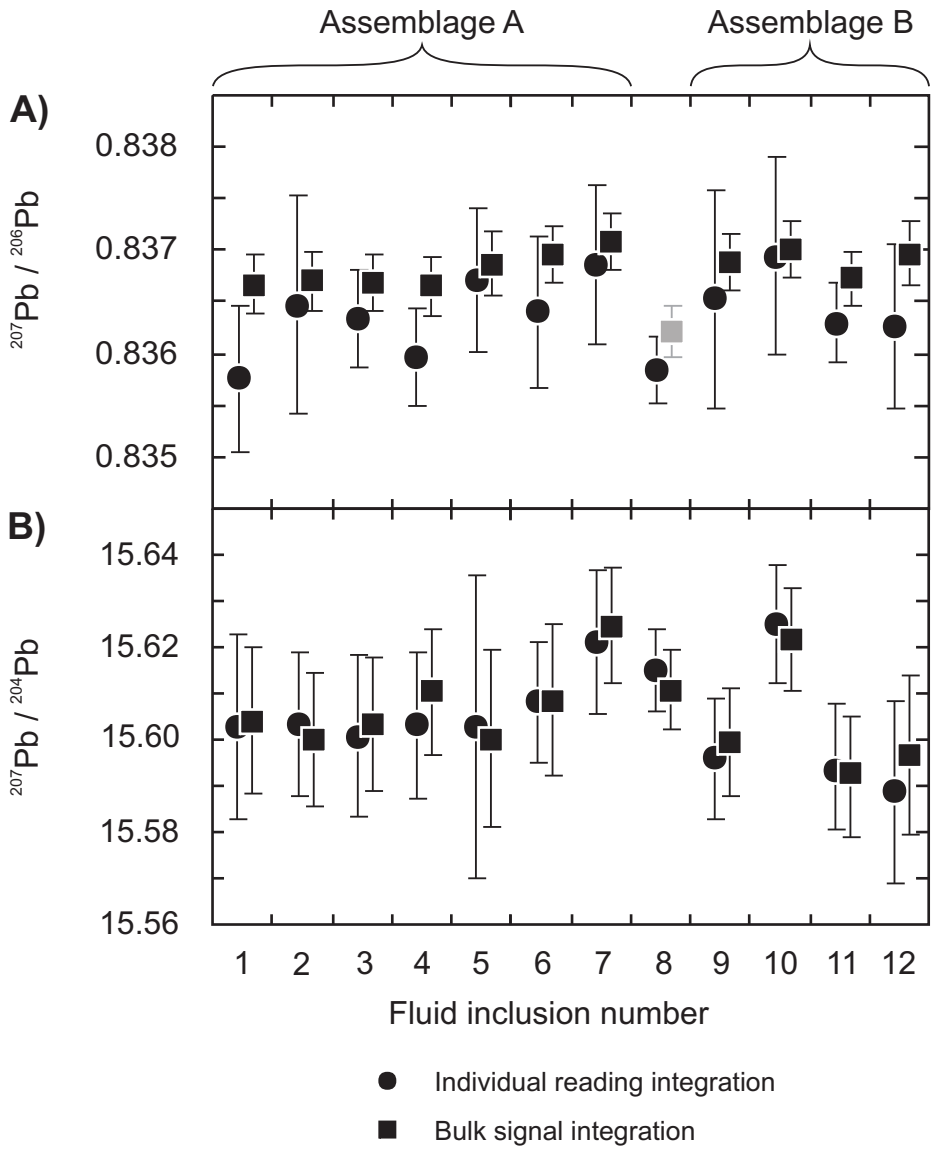
Assemblage A
Assemblage B
A)
B)
$^{207}Pb / ^{206}Pb$
$^{207}Pb / ^{204}Pb$
0.838
0.837
0.836
0.835
15.64
15.62
15.60
15.58
15.56
1 2 3 4 5 6 7 8 9 10 11 12
Fluid inclusion number
Individual reading integration
Bulk signal integration

Figure 8

Table A1: LA-ICPMS data for SRM 610 glass acquired during this study

Run	Comments	Pb/Tl measured	$^{208}Pb/^{206}Pb$ final	1 SE abs	Readings integrated	$^{207}Pb/^{206}Pb$ final	1 SE abs	Readings integrated	$^{206}Pb/^{204}Pb$ final	1 SE abs	Readings integrated	$^{207}Pb/^{204}Pb$ final	1 SE abs	Readings integrated	$^{208}Pb/^{204}Pb$ final	1 SE abs	Readings integrated
SRM 610 reference values (Baker et al., 2004)			2.1694			0.90986			17.052			15.515			36.991		
Nu Plasma 1700																	
April 28, 2003																	
2SRM610	90s, 1 µm/s, 98mJ, 6Hz, 60µm pit	6.1	2.16938	0.00012	359 of 366	0.90986	0.00003	363 of 366	17.050	0.002	354 of 366	15.513	0.002	353 of 366	36.986	0.005	354 of 366
22SRM610	90s, 1 µm/s, 98mJ, 6Hz, 60µm pit	6.1	2.16962	0.00012	339 of 354	0.90991	0.00003	340 of 354	17.056	0.002	339 of 354	15.520	0.002	336 of 354	37.003	0.004	333 of 354
222SRM610	90s, 1 µm/s, 98mJ, 6Hz, 60µm pit	6.1	2.16946	0.00012	384 of 402	0.90989	0.00003	384 of 402	17.051	0.002	383 of 402	15.516	0.002	381 of 402	36.994	0.005	386 of 402
3SRM610	90s, 1 µm/s, 98mJ, 6Hz, 60µm pit	6.1	2.16943	0.00012	398 of 417	0.90989	0.00003	401 of 417	17.054	0.001	397 of 417	15.518	0.002	397 of 417	37.000	0.004	396 of 417
4SRM610	90s, 1 µm/s, 98mJ, 6Hz, 60µm pit	6.1	2.16954	0.00011	369 of 394	0.90990	0.00003	376 of 394	17.053	0.002	378 of 394	15.517	0.002	374 of 394	36.995	0.004	377 of 394
5SRM610	90s, 1 µm/s, 60mJ, 6Hz, 60µm pit	6.1	2.16965	0.00015	393 of 409	0.90988	0.00004	391 of 409	17.055	0.002	386 of 409	15.518	0.002	390 of 409	36.998	0.005	391 of 409
6SRM610	90s, 1 µm/s, 60mJ, 6Hz, 60µm pit	6.1	2.16960	0.00014	389 of 407	0.90988	0.00004	391 of 407	17.052	0.002	385 of 407	15.516	0.002	392 of 407	36.994	0.005	390 of 407
66SRM610	90s, 1 µm/s, 60mJ, 6Hz, 60µm pit	6.2	2.16918	0.00014	392 of 407	0.90981	0.00004	386 of 407	17.053	0.002	389 of 407	15.515	0.002	388 of 407	36.990	0.005	388 of 407
7SRM610	90s, ONE SPOT, 60mJ, 6Hz, 60µm pit	6.7	2.16901	0.00014	385 of 406	0.90978	0.00004	386 of 406	17.048	0.002	393 of 406	15.511	0.002	392 of 406	36.978	0.006	392 of 406
77SRM610	90s, ONE SPOT, 60mJ, 6Hz, 60µm pit	6.8	2.16892	0.00015	396 of 414	0.90978	0.00004	391 of 414	17.048	0.002	392 of 414	15.510	0.002	396 of 414	36.974	0.006	396 of 414
8SRM610	90s, 1 µm/s, 60mJ, 6Hz, 120µm pit	8.1	2.16913	0.00007	781 of 818	0.90982	0.00002	781 of 818	17.048	0.001	790 of 818	15.510	0.001	785 of 818	36.976	0.002	781 of 818
9SRM610	90s, 1 µm/s, 100mJ, 6Hz, 120µm pit	8.8	2.16992	0.00005	821 of 840	0.90998	0.00001	822 of 840	17.055	0.001	817 of 840	15.520	0.001	824 of 840	37.006	0.002	823 of 840
99SRM610	90s, 1 µm/s, 120mJ, 6Hz, 120µm pit	8.4	2.16968	0.00005	827 of 866	0.90993	0.00001	819 of 866	17.053	0.000	831 of 866	15.517	0.000	824 of 866	36.998	0.001	831 of 866
11SRM610	90s, 1 µm/s, 50mJ, 10Hz, 120µm pit	6.8	2.16884	0.00007	768 of 803	0.90976	0.00002	769 of 803	17.047	0.001	766 of 803	15.509	0.001	765 of 803	36.970	0.002	765 of 803
	average		**2.16938**			**0.90986**			**17.0517**			**15.5149**			**36.9902**		
	1 SD (abs)		**0.00032**			**0.00006**			**0.0031**			**0.0037**			**0.0115**		
	1 SD (ppm)		148			71			181			239			312		
August 26, 2004																	
04_SRM610_Aug26_04	90s, 1 µm/s, 98mJ, 6Hz, 60µm pit	7.6	2.16992	0.00028	350 of 367	0.90990	0.00007	349 of 367	17.056	0.004	355 of 367	15.520	0.004	353 of 367	37.006	0.011	354 of 367
05_SRM610_Aug26_04	90s, 1 µm/s, 98mJ, 6Hz, 60µm pit	6.6	2.16954	0.00031	387 of 406	0.90982	0.00007	387 of 406	17.067	0.004	389 of 406	15.527	0.004	390 of 406	37.023	0.011	386 of 406
06_SRM610_Aug26_04	90s, 1 µm/s, 98mJ, 6Hz, 60µm pit	*6.6*	2.16924	0.00026	340 of 354	0.90979	0.00006	336 of 354	17.068	0.004	337 of 354	15.529	0.004	338 of 354	37.024	0.011	341 of 354
07_SRM610_Aug26_04	*90s, 1 µm/s, 98mJ, 6Hz, 60µm pit*	*21.1*	*2.16803*	*0.00063*	*338 of 353*	*0.90952*	*0.00013*	*337 of 353*	*17.051*	*0.006*	*341 of 353*	*15.508*	*0.007*	*337 of 353*	*36.966*	*0.022*	*337 of 353*
08_SRM610_Aug26_04	*90s, 1 µm/s, 98mJ, 6Hz, 60µm pit*	*33.7*	*2.17249*	*0.00093*	*352 of 365*	*0.91043*	*0.00020*	*354 of 365*	*17.089*	*0.008*	*348 of 365*	*15.558*	*0.010*	*347 of 365*	*37.120*	*0.032*	*351 of 365*
09_SRM610_Aug26_04	*90s, 1 µm/s, 98mJ, 6Hz, 60µm pit*	*23.8*	*2.16949*	*0.00058*	*351 of 368*	*0.90982*	*0.00013*	*350 of 368*	*17.057*	*0.006*	*354 of 368*	*15.519*	*0.007*	*353 of 368*	*37.004*	*0.020*	*352 of 368*
10_SRM610_Aug26_04	90s, 1 µm/s, 98mJ, 6Hz, 60µm pit	6.1	2.16941	0.00025	338 of 358	0.90976	0.00006	338 of 358	17.059	0.004	345 of 358	15.522	0.004	347 of 358	37.012	0.011	344 of 358
11_SRM610_Aug26_04	90s, 1 µm/s, 98mJ, 6Hz, 60µm pit	6.1	2.16946	0.00028	325 of 341	0.90982	0.00007	326 of 341	17.060	0.005	322 of 341	15.522	0.005	323 of 341	37.012	0.012	325 of 341
12_SRM610_Aug26_04	90s, 1 µm/s, 98mJ, 6Hz, 60µm pit	6.1	2.16970	0.00023	350 of 367	0.90990	0.00006	352 of 367	17.064	0.004	351 of 367	15.527	0.004	351 of 367	37.023	0.010	354 of 367
13_SRM610_Aug26_04	90s, 1 µm/s, 98mJ, 6Hz, 60µm pit	6.6	2.16953	0.00026	361 of 376	0.90988	0.00006	357 of 376	17.047	0.004	357 of 376	15.512	0.004	357 of 376	36.981	0.012	361 of 376
14_SRM610_Aug26_04	90s, 1 µm/s, 98mJ, 6Hz, 60µm pit	6.6	2.16939	0.00029	344 of 358	0.90988	0.00007	343 of 358	17.067	0.004	341 of 358	15.531	0.004	342 of 358	37.029	0.011	343 of 358
15_SRM610_Aug26_04	90s, 1 µm/s, 98mJ, 6Hz, 60µm pit	6.6	2.16922	0.00032	312 of 330	0.90987	0.00008	317 of 330	17.062	0.005	312 of 330	15.524	0.005	311 of 330	37.008	0.013	313 of 330
16_SRM610_Aug26_04	90s, 1 µm/s, 98mJ, 6Hz, 60µm pit	6.6	2.17012	0.00031	352 of 370	0.90992	0.00007	351 of 370	17.060	0.004	353 of 370	15.522	0.004	349 of 370	37.021	0.012	349 of 370
17_SRM610_Aug26_04	90s, 1 µm/s, 98mJ, 6Hz, 60µm pit	6.3	2.16970	0.00029	337 of 353	0.90985	0.00007	341 of 353	17.052	0.004	340 of 353	15.513	0.004	336 of 353	36.991	0.012	336 of 353
18_SRM610_Aug26_04	90s, 1 µm/s, 98mJ, 6Hz, 60µm pit	6.2	2.16926	0.00026	363 of 380	0.90983	0.00006	358 of 380	17.062	0.004	362 of 380	15.522	0.004	365 of 380	37.007	0.011	360 of 380
19_SRM610_Aug26_04	90s, 1 µm/s, 98mJ, 6Hz, 60µm pit	6.1	2.16953	0.00031	356 of 370	0.90976	0.00008	353 of 370	17.073	0.005	355 of 370	15.532	0.005	357 of 370	37.037	0.012	353 of 370
20_SRM610_Aug26_04	90s, 1 µm/s, 98mJ, 6Hz, 60µm pit	6.1	2.16881	0.00026	341 of 363	0.90969	0.00006	343 of 363	17.049	0.004	352 of 363	15.510	0.004	350 of 363	36.976	0.011	351 of 363
21_SRM610_Aug26_04	90s, 1 µm/s, 98mJ, 6Hz, 60µm pit	*9.2*	2.16970	0.00037	342 of 360	0.90981	0.00009	345 of 360	17.070	0.004	344 of 360	15.530	0.004	345 of 360	37.033	0.012	343 of 360
22_SRM610_Aug26_04	*90s, 1 µm/s, 98mJ, 6Hz, 60µm pit*	6.5	*2.17080*	*0.00041*	*367 of 379*	*0.91010*	*0.00010*	*367 of 379*	*17.078*	*0.005*	*363 of 379*	*15.542*	*0.005*	*364 of 379*	*37.073*	*0.015*	*362 of 379*
23_SRM610_Aug26_04	90s, 1 µm/s, 98mJ, 6Hz, 60µm pit	6.0	2.17022	0.00026	343 of 360	0.90994	0.00006	344 of 360	17.054	0.004	344 of 360	15.519	0.004	345 of 360	37.015	0.011	344 of 360
24_SRM610_Aug26_04	90s, 1 µm/s, 98mJ, 6Hz, 60µm pit	6.1	2.16935	0.00028	322 of 335	0.90987	0.00007	323 of 335	17.059	0.005	322 of 335	15.521	0.005	321 of 335	37.008	0.012	320 of 335
	average		**2.16966**			**0.90987**			**17.0620**			**15.5243**			**37.0175**		
	1 SD (abs)		**0.00084**			**0.00017**			**0.0100**			**0.0112**			**0.0328**		
	1 SD (ppm)		388			185			585			718			886		
November 05, 2004																	
test_3_Nov05_04	90s, 1 µm/s, 98mJ, 6Hz, 60µm pit	6.5	2.16913	0.00023	360 of 380	0.90977	0.00006	359 of 380	17.055	0.002	365 of 380	15.517	0.002	363 of 380	36.994	0.007	363 of 380
test_4_Nov05_04	90s, 1 µm/s, 98mJ, 6Hz, 60µm pit	6.2	2.16892	0.00022	359 of 378	0.90971	0.00005	357 of 378	17.054	0.002	362 of 378	15.513	0.002	362 of 378	36.987	0.007	360 of 378
test_5_Nov05_04	90s, 1 µm/s, 98mJ, 6Hz, 60µm pit	6.3	2.16904	0.00024	331 of 350	0.90974	0.00006	332 of 350	17.049	0.002	338 of 350	15.512	0.002	335 of 350	36.978	0.007	333 of 350
test_6_Nov05_04	90s, 1 µm/s, 98mJ, 6Hz, 60µm pit	6.3	2.16951	0.00024	366 of 388	0.90986	0.00006	367 of 388	17.058	0.002	369 of 388	15.520	0.002	369 of 388	37.004	0.007	370 of 388
test_7_Nov05_04	90s, 1 µm/s, 98mJ, 6Hz, 60µm pit	6.4	2.16917	0.00025	362 of 376	0.90984	0.00006	361 of 376	17.050	0.002	356 of 376	15.514	0.002	360 of 376	36.986	0.007	355 of 376
test_8_Nov05_04	90s, 1 µm/s, 98mJ, 6Hz, 60µm pit	6.6	2.16892	0.00022	355 of 374	0.90969	0.00006	357 of 374	17.048	0.002	359 of 374	15.508	0.003	364 of 374	36.972	0.007	360 of 374
test_9_Nov05_04	90s, 1 µm/s, 98mJ, 6Hz, 60µm pit	6.6	2.16915	0.00020	361 of 377	0.90977	0.00005	359 of 377	17.046	0.002	361 of 377	15.509	0.002	360 of 377	36.972	0.007	360 of 377
test_10_Nov05_04	90s, 1 µm/s, 98mJ, 6Hz, 60µm pit	6.2	2.16895	0.00025	347 of 369	0.90974	0.00006	352 of 369	17.043	0.002	353 of 369	15.504	0.002	349 of 369	36.963	0.007	349 of 369
	average		**2.16910**			**0.90977**			**17.0503**			**15.5120**			**36.9820**		
	1 SD (abs)		**0.00019**			**0.00006**			**0.0049**			**0.0050**			**0.0134**		
	1 SD (ppm)		90			65			285			323			362		

November06, 2004																
Nov_06_01	90s, 1 µm/s, 100mJ, 6Hz, 60µm pit	6.1	2.16891	0.00024	361 of 375	0.90982	0.00006	360 of 375	17.050	0.002	355 of 375	15.514	0.002	356 of 375	36.984	0.006	361 of 375
Nov_06_02	90s, 1 µm/s, 100mJ, 6Hz, 60µm pit	6.0	2.16936	0.00025	365 of 378	0.90987	0.00006	360 of 378	17.049	0.002	361 of 378	15.512	0.002	362 of 378	36.985	0.006	359 of 378
Nov_06_03	90s, 1 µm/s, 100mJ, 6Hz, 60µm pit	6.1	2.16924	0.00024	360 of 373	0.90982	0.00006	357 of 373	17.051	0.002	354 of 373	15.513	0.002	355 of 373	36.986	0.006	356 of 373
	average		**2.16917**			**0.90983**			**17.0502**			**15.5132**			**36.9850**		
	1 SD (abs)		**0.00023**			**0.00003**			**0.0008**			**0.0006**			**0.0006**		
	1 SD (ppm)		108			31			48			39			17		
Nov_06_04	90s, 1 µm/s, 100mJ, 6Hz, 60µm pit	7.9	2.16933	0.00028	369 of 385	0.90984	0.00007	373 of 385	17.053	0.002	369 of 385	15.516	0.003	367 of 385	36.991	0.008	370 of 385
Nov_06_05	90s, 1 µm/s, 100mJ, 6Hz, 60µm pit	8.9	2.16991	0.00026	376 of 394	0.90998	0.00006	378 of 394	17.058	0.002	376 of 394	15.522	0.003	377 of 394	37.010	0.007	375 of 394
Nov_06_06	*90s, 1 µm/s, 100mJ, 6Hz, 60µm pit*	*13.9*	*2.16611*	*0.00032*	*357 of 378*	*0.90926*	*0.00007*	*360 of 378*	*17.024*	*0.002*	*356 of 378*	*15.478*	*0.003*	*364 of 378*	*36.871*	*0.009*	*362 of 378*
	average		**2.16962**			**0.90991**			**17.0554**			**15.5190**			**37.0002**		
	1 SD (abs)		**0.00040**			**0.00010**			**0.0030**			**0.0047**			**0.0132**		
	1 SD (ppm)		186			112			177			300			357		
Nov_06_20	90s, 1 µm/s, 100mJ, 6Hz, 60µm pit	6.3	2.16910	0.00034	344 of 367	0.90984	0.00008	343 of 367	17.050	0.002	345 of 367	15.513	0.003	347 of 367	36.980	0.009	349 of 367
Nov_06_21	90s, 1 µm/s, 100mJ, 6Hz, 60µm pit	6.2	2.16945	0.00030	350 of 372	0.90993	0.00007	348 of 372	17.053	0.002	356 of 372	15.516	0.003	359 of 372	36.993	0.009	354 of 372
Nov_06_22	90s, 1 µm/s, 100mJ, 6Hz, 60µm pit	6.2	2.16970	0.00035	363 of 376	0.90991	0.00008	360 of 376	17.049	0.002	359 of 376	15.512	0.003	362 of 376	36.986	0.008	357 of 376
	average		**2.16941**			**0.90989**			**17.0510**			**15.5138**			**36.9864**		
	1 SD (abs)		**0.00030**			**0.00005**			**0.0022**			**0.0019**			**0.0066**		
	1 SD (ppm)		139			50			130			124			177		
Nov_06_30	90s, 1 µm/s, 100mJ, 6Hz, 60µm pit	6.6	2.16889	0.00032	338 of 358	0.90981	0.00008	337 of 358	17.042	0.002	346 of 358	15.503	0.003	342 of 358	36.955	0.008	342 of 358
Nov_06_31	90s, 1 µm/s, 100mJ, 6Hz, 60µm pit	6.5	2.16882	0.00029	343 of 365	0.90980	0.00007	348 of 365	17.047	0.002	344 of 365	15.510	0.002	349 of 365	36.973	0.007	348 of 365
Nov_06_32	90s, 1 µm/s, 100mJ, 6Hz, 60µm pit	7.7	2.16917	0.00031	336 of 357	0.90990	0.00007	335 of 357	17.046	0.002	346 of 357	15.508	0.003	346 of 357	36.971	0.008	345 of 357
	average		**2.16896**			**0.90984**			**17.045**			**15.507**			**36.967**		
	1 SD (abs)		**0.00019**			**0.00005**			**0.003**			**0.003**			**0.010**		
	1 SD (ppm)		86			59			165			214			263		
Daily average (November 06)			**2.16926**			**0.90987**			**17.050**			**15.513**			**36.983**		
	2 SD (abs)		**0.00068**			**0.00012**			**0.008**			**0.010**			**0.028**		
	2SD (ppm)		313			128			491			617			747		
	2SE (ppm)		74			30			116			145			176		
June 07, 2005																
June07_SRM610_a	90s, 1 µm/s, 100mJ, 6Hz, 60µm pit	6.2	2.16980	0.00021	226 of 234	0.90994	0.00005	227 of 234	17.056	0.003	224 of 234	15.520	0.003	225 of 234	37.008	0.009	227 of 234
June07_SRM610_b	90s, 1 µm/s, 100mJ, 6Hz, 60µm pit	6.2	2.16978	0.00019	240 of 253	0.91002	0.00004	240 of 253	17.049	0.003	242 of 253	15.515	0.003	242 of 253	36.994	0.007	242 of 253
June07_SRM610_c	90s, 1 µm/s, 100mJ, 6Hz, 60µm pit	6.2	2.16981	0.00020	237 of 250	0.90994	0.00005	238 of 250	17.059	0.003	236 of 250	15.521	0.003	239 of 250	37.009	0.008	239 of 250
June07_SRM610_d	90s, 1 µm/s, 100mJ, 6Hz, 60µm pit	6.8	2.17002	0.00023	224 of 235	0.90995	0.00006	228 of 235	17.053	0.003	226 of 235	15.518	0.003	224 of 235	37.005	0.008	225 of 235
June07_SRM610_e	90s, 1 µm/s, 100mJ, 6Hz, 60µm pit	6.8	2.16987	0.00021	238 of 256	0.90991	0.00005	244 of 256	17.046	0.003	243 of 256	15.511	0.003	242 of 256	36.986	0.008	243 of 256
June07_SRM610_f	90s, 1 µm/s, 100mJ, 6Hz, 60µm pit	6.7	2.17003	0.00020	236 of 245	0.90995	0.00005	234 of 245	17.053	0.003	236 of 245	15.517	0.003	237 of 245	37.005	0.008	234 of 245
	average		**2.16988**			**0.90995**			**17.0526**			**15.5171**			**37.0012**		
	1 SD (abs)		**0.00011**			**0.00004**			**0.0046**			**0.0034**			**0.0093**		
	1 SD (ppm)		52			42			271			220			252		
June 08, 2005																
June08_SRM610_a	90s, 1 µm/s, 100mJ, 6Hz, 60µm pit	6.2	2.16957	0.00030	241 of 253	0.90994	0.00007	241 of 253	17.053	0.002	244 of 253	15.516	0.002	247 of 253	36.995	0.007	245 of 253
June08_SRM610_b	90s, 1 µm/s, 100mJ, 6Hz, 60µm pit	6.1	2.17013	0.00016	237 of 245	0.91003	0.00004	233 of 245	17.058	0.002	235 of 245	15.523	0.002	236 of 245	37.018	0.006	237 of 245
June08_SRM610_c	90s, 1 µm/s,90mJ, 6Hz, 60µm pit	6.1	2.16988	0.00024	244 of 258	0.90995	0.00006	247 of 258	17.053	0.002	248 of 258	15.516	0.002	249 of 258	36.997	0.007	248 of 258
June08_SRM610_d	90s, 1 µm/s,90mJ, 6Hz, 60µm pit	6.1	2.16980	0.00017	241 of 249	0.91002	0.00004	241 of 249	17.048	0.002	235 of 249	15.514	0.002	237 of 249	36.987	0.006	237 of 249
June08_SRM610_e	90s, 1 µm/s,80mJ, 6Hz, 60µm pit	6.0	2.16949	0.00016	230 of 240	0.90987	0.00004	229 of 240	17.047	0.002	229 of 240	15.512	0.002	230 of 240	36.984	0.006	232 of 240
June08_SRM610_f	90s, 1 µm/s,80mJ, 6Hz, 60µm pit	6.2	2.16986	0.00022	247 of 260	0.90999	0.00005	247 of 260	17.054	0.002	249 of 260	15.520	0.002	247 of 260	37.001	0.006	247 of 260
June08_SRM610_g	90s, 1 µm/s, 70mJ, 6Hz, 60µm pit	6.2	2.16990	0.00025	220 of 232	0.91001	0.00006	222 of 232	17.054	0.002	221 of 232	15.519	0.002	219 of 232	37.004	0.006	217 of 232
June08_SRM610_h	90s, 1 µm/s, 70mJ, 6Hz, 60µm pit	6.1	2.16990	0.00023	247 of 261	0.90999	0.00006	247 of 261	17.054	0.002	249 of 261	15.520	0.002	248 of 261	37.007	0.007	247 of 261
June08_SRM610_i	90s, 1 µm/s, 50mJ, 6Hz, 60µm pit	6.0	2.16971	0.00023	240 of 254	0.91004	0.00005	239 of 254	17.052	0.002	246 of 254	15.517	0.002	244 of 254	37.001	0.007	244 of 254
June08_SRM610_k	90s, 1 µm/s, 50mJ, 6Hz, 60µm pit	6.1	2.16991	0.00023	256 of 268	0.90994	0.00006	257 of 268	17.055	0.002	253 of 268	15.519	0.003	254 of 268	37.010	0.007	259 of 268
	average		**2.16982**			**0.90998**			**17.0528**			**15.5176**			**37.0003**		
	1 SD (abs)		**0.00018**			**0.00005**			**0.0034**			**0.0034**			**0.0101**		
	1 SD (ppm)		85			58			197			220			273		

August 30, 2005																
SRM610_Aug30-05_1	90s, 1 µm/s, 100mJ, 6Hz, 60µm pit	6.6	2.16932	0.00015	307 of 323	0.90988	0.00004	307 of 323	17.050	0.002	310 of 323	15.514	0.002	311 of 323	36.984	0.005	311 of 323
SRM610_Aug30-05_2	90s, 1 µm/s, 100mJ, 6Hz, 60µm pit	6.5	2.16919	0.00014	295 of 312	0.90987	0.00004	299 of 312	17.051	0.002	300 of 312	15.514	0.002	298 of 312	36.985	0.005	297 of 312
SRM610_Aug30-05_3	90s, 1 µm/s, 100mJ, 6Hz, 60µm pit	6.3	2.16908	0.00016	266 of 280	0.90978	0.00004	269 of 280	17.048	0.002	266 of 280	15.510	0.002	269 of 280	36.978	0.006	268 of 280
	average		**2.16920**			**0.90984**			**17.0497**			**15.5124**			**36.9823**		
	1 SD (abs)		**0.00012**			**0.00005**			**0.0011**			**0.0023**			**0.0036**		
	1 SD (ppm)		55			60			66			147			99		
SRM610_Aug30-05_4	90s, 1 µm/s, 70mJ, 6Hz, 60µm pit	6.7	2.16910	0.00015	307 of 319	0.90978	0.00004	309 of 319	17.046	0.002	305 of 319	15.507	0.002	306 of 319	36.970	0.005	306 of 319
SRM610_Aug30-05_5	90s, 1 µm/s, 70mJ, 6Hz, 60µm pit	6.7	2.16920	0.00014	287 of 305	0.90977	0.00004	290 of 305	17.052	0.002	293 of 305	15.512	0.002	293 of 305	36.985	0.005	294 of 305
SRM610_Aug30-05_6	90s, 1 µm/s, 70mJ, 6Hz, 60µm pit	6.8	2.16912	0.00015	323 of 343	0.90976	0.00004	319 of 343	17.048	0.002	324 of 343	15.510	0.002	327 of 343	36.979	0.005	325 of 343
	average		**2.16914**			**0.90977**			**17.0486**			**15.5098**			**36.9779**		
	1 SD (abs)		**0.00005**			**0.00001**			**0.0029**			**0.0024**			**0.0078**		
	1 SD (ppm)		24			8			171			154			212		
SRM610_Aug30-05_7	90s, 1 µm/s, 70mJ, 6Hz, 60µm pit	6.0	2.16935	0.00013	309 of 322	0.90986	0.00003	307 of 322	17.052	0.002	309 of 322	15.514	0.002	307 of 322	36.989	0.005	307 of 322
SRM610_Aug30-05_8	90s, 1 µm/s, 70mJ, 6Hz, 60µm pit	6.1	2.16905	0.00014	320 of 340	0.90982	0.00004	322 of 340	17.049	0.002	328 of 340	15.511	0.002	329 of 340	36.978	0.005	328 of 340
SRM610_Aug30-05_9	90s, 1 µm/s, 70mJ, 6Hz, 60µm pit	6.2	2.16923	0.00013	311 of 327	0.90980	0.00003	310 of 327	17.047	0.002	314 of 327	15.510	0.002	312 of 327	36.978	0.005	309 of 327
	average		**2.16921**			**0.90983**			**17.0496**			**15.5116**			**36.9814**		
	1 SD (abs)		**0.00015**			**0.00003**			**0.0024**			**0.0024**			**0.0064**		
	1 SD (ppm)		70			32			143			156			174		
SRM610_Aug30-05_10	90s, 1 µm/s, 70mJ, 6Hz, 60µm pit	6.7	2.16921	0.00016	250 of 261	0.90982	0.00004	248 of 261	17.046	0.002	251 of 261	15.509	0.002	252 of 261	36.971	0.006	252 of 261
SRM610_Aug30-05_11	90s, 1 µm/s, 70mJ, 6Hz, 60µm pit	6.8	2.16933	0.00015	281 of 291	0.90989	0.00004	281 of 291	17.048	0.002	278 of 291	15.512	0.002	278 of 291	36.980	0.006	277 of 291
SRM610_Aug30-05_12	90s, 1 µm/s, 70mJ, 6Hz, 60µm pit	6.4	2.16924	0.00015	275 of 286	0.90982	0.00004	272 of 286	17.049	0.002	277 of 286	15.511	0.002	272 of 286	36.978	0.005	272 of 286
	average		**2.16926**			**0.90984**			**17.0477**			**15.5105**			**36.9764**		
	1 SD (abs)		**0.00006**			**0.00004**			**0.0014**			**0.0015**			**0.0044**		
	1 SD (ppm)		28			43			85			99			120		
SRM610_Aug30-05_13	90s, 1 µm/s, 70mJ, 6Hz, 60µm pit	6.8	2.16922	0.00013	324 of 338	0.90983	0.00003	320 of 338	17.046	0.002	322 of 338	15.508	0.002	319 of 338	36.972	0.005	319 of 338
SRM610_Aug30-05_14	90s, 1 µm/s, 70mJ, 6Hz, 60µm pit	6.8	2.16937	0.00014	316 of 326	0.90991	0.00004	311 of 326	17.046	0.002	310 of 326	15.510	0.002	310 of 326	36.974	0.005	307 of 326
SRM610_Aug30-05_15	90s, 1 µm/s, 70mJ, 6Hz, 60µm pit	6.1	2.16928	0.00013	317 of 332	0.90987	0.00003	317 of 332	17.047	0.002	314 of 332	15.511	0.002	311 of 332	36.976	0.005	312 of 332
	average		**2.16929**			**0.90987**			**17.0463**			**15.5096**			**36.9741**		
	1 SD (abs)		**0.00008**			**0.00004**			**0.0008**			**0.0013**			**0.0019**		
	1 SD (ppm)		35			40			44			81			52		
SRM610_Aug30-05_16	90s, 1 µm/s, 70mJ, 6Hz, 60µm pit	6.0	2.16953	0.00012	334 of 350	0.90992	0.00003	336 of 350	17.045	0.002	333 of 350	15.511	0.002	334 of 350	36.979	0.005	336 of 350
SRM610_Aug30-05_17	90s, 1 µm/s, 70mJ, 6Hz, 60µm pit	6.5	2.16910	0.00013	313 of 331	0.90980	0.00004	320 of 331	17.044	0.002	321 of 331	15.507	0.002	319 of 331	36.965	0.005	319 of 331
SRM610_Aug30-05_18	90s, 1 µm/s, 70mJ, 6Hz, 60µm pit	6.5	2.16942	0.00012	330 of 343	0.90984	0.00003	335 of 343	17.041	0.002	327 of 343	15.506	0.002	331 of 343	36.969	0.005	329 of 343
	average		**2.16935**			**0.90985**			**17.0436**			**15.5076**			**36.9712**		
	1 SD (abs)		**0.00022**			**0.00006**			**0.0019**			**0.0027**			**0.0070**	137.967	
	1 SD (ppm)		103			69			109			174			190		
Daily average (August 30)			**2.16924**			**0.90984**			**17.048**			**15.510**			**36.977**		
	1 SD (abs)		**0.00013**			**0.00005**			**0.00271**			**0.00241**			**0.00617**		
	1 SD (ppm)		59			53			159			155			167		
	1 SE (ppm)		14			12			38			37			39		
Nu 1700 grand average			**2.16943**			**0.90986**			**17.052**			**15.515**			**36.992**		
	1 SD (abs)		**0.00035**			**0.00008**			**0.00624**			**0.00613**			**0.01737**		
	1 SD (ppm)		160			87			366			395			470		
	1 SE (ppm)		17			9			40			43			51		

Nu Plasma

April 09, 2003																	
2SRM610	90s, 1 µm/s, 98mJ, 6Hz, 60µm pit	6.4	2.16935	0.00026	383 of 402	0.90981	0.00007	382 of 402	17.070	0.005	383 of 402	15.531	0.005	383 of 402	37.031	0.012	382 of 402
3SRM610	90s, 1 µm/s, 98mJ, 6Hz, 60µm pit	5.9	2.16887	0.00026	318 of 334	0.90972	0.00007	318 of 334	17.072	0.006	320 of 334	15.527	0.006	320 of 334	37.019	0.014	318 of 334
4SRM610	90s, 1 µm/s, 98mJ, 6Hz, 60µm pit	5.8	2.16922	0.00025	353 of 369	0.90981	0.00007	355 of 369	17.066	0.006	353 of 369	15.526	0.005	353 of 369	37.018	0.013	353 of 369
5NIST610	90s, 1 µm/s, 50mJ, 6Hz, 60µm pit	*5.9*	2.16922	0.00036	360 of 375	0.90980	0.00009	360 of 375	17.066	0.008	353 of 375	15.525	0.007	357 of 375	37.015	0.019	356 of 375
6SRM610	90s, 1 µm/s, 50mJ, 6Hz, 60µm pit	6.0	2.16954	0.00041	297 of 311	0.90986	0.00009	294 of 311	17.078	0.009	299 of 311	15.539	0.008	297 of 311	37.049	0.020	296 of 311
7SRM610	*90s, one spot, 50mJ, 6Hz, 60µm pit*	*16.0*	*2.16627*	*0.00014*	*385 of 406*	*0.90926*	*0.00004*	*386 of 406*	*17.027*	*0.002*	*393 of 406*	*15.482*	*0.002*	*392 of 406*	*36.884*	*0.006*	*392 of 406*
8SRM610	180s, one spot, 50mJ, 6Hz, 120µm pit	5.6	2.16884	0.00011	771 of 805	0.90971	0.00003	776 of 805	17.055	0.003	773 of 805	15.515	0.002	768 of 805	36.987	0.006	768 of 805
9SRM610	180s, one spot, 100mJ, 6Hz, 120µm pit	5.7	2.16931	0.00007	766 of 808	0.90983	0.00003	775 of 808	17.060	0.002	776 of 808	15.522	0.001	767 of 808	37.007	0.004	771 of 808
10SRM610	180s, one spot, 100mJ, 2Hz, 120µm pit	5.6	2.16922	0.00015	802 of 837	0.90978	0.00005	800 of 837	17.073	0.004	794 of 837	15.532	0.003	795 of 837	37.031	0.008	793 of 837
11SRM610	180s, one spot, 50mJ, 10Hz, 120µm pit	5.6	2.16896	0.00008	779 of 813	0.90972	0.00003	766 of 813	17.053	0.002	777 of 813	15.513	0.002	778 of 813	36.983	0.004	780 of 813
	average		**2.16888**			**0.90973**			**17.0620**			**15.5211**			**37.0024**		
	1 SD (abs)		**0.00094**			**0.00017**			**0.0146**			**0.0157**			**0.0460**		
	1 SD (ppm)		435			190			858			1011			1244		
August 22, 2004																	
01 SRM610	90s, 1 µm/s, 100mJ, 6Hz, 60µm pit	6.4	2.16959	0.00020	234 of 242	0.90989	0.00005	231 of 242	17.072	0.004	228 of 242	15.533	0.003	229 of 242	37.036	0.008	233 of 242
02 SRM610	90s, 1 µm/s, 100mJ, 6Hz, 60µm pit	6.3	2.16959	0.00019	232 of 248	0.90989	0.00005	238 of 248	17.063	0.005	239 of 248	15.523	0.005	240 of 248	37.015	0.011	238 of 248
03 NIST610	90s, 1 µm/s, 100mJ, 6Hz, 60µm pit	6.4	2.17003	0.00025	209 of 220	0.90993	0.00006	208 of 220	17.059	0.005	209 of 220	15.524	0.005	212 of 220	37.017	0.011	212 of 220
	average		**2.16973**			**0.90991**			**17.0648**			**15.5266**			**37.0227**		
	1 SD (abs)		**0.00025**			**0.00002**			**0.0068**			**0.0055**			**0.0117**		
	1 SD (ppm)		117			27			399			355			315		
August 23 2004																	
SRM610_1	90s, 1 µm/s, 100mJ, 6Hz, 60µm pit	6.7	2.16988	0.00017	330 of 349	0.90996	0.00004	326 of 349	17.056	0.004	332 of 349	15.519	0.003	330 of 349	37.006	0.007	328 of 349
SRM610_2	90s, 1 µm/s, 100mJ, 6Hz, 60µm pit	6.8	2.17000	0.00022	314 of 330	0.91003	0.00006	315 of 330	17.062	0.004	317 of 330	15.527	0.004	319 of 330	37.022	0.009	319 of 330
	average		**2.16994**			**0.90999**			**17.0591**			**15.5228**			**37.0140**		
	1 SD (abs)		**0.00009**			**0.00005**			**0.0041**			**0.0059**			**0.0118**		
	1 SD (ppm)		41			54			239			383			318		
SRM610_20	90s, 1 µm/s, 100mJ, 6Hz, 60µm pit	6.3	2.17007	0.00021	361 of 379	0.91001	0.00005	356 of 379	17.063	0.005	367 of 379	15.527	0.005	368 of 379	37.023	0.011	365 of 379
SRM610_21	90s, 1 µm/s, 100mJ, 6Hz, 60µm pit	6.4	2.16976	0.00015	363 of 382	0.90995	0.00004	363 of 382	17.047	0.003	368 of 382	15.513	0.003	366 of 382	36.988	0.007	362 of 382
SRM610_22	90s, 1 µm/s, 100mJ, 6Hz, 60µm pit	6.4	2.16981	0.00015	371 of 392	0.90994	0.00004	373 of 392	17.044	0.003	373 of 392	15.510	0.003	371 of 392	36.985	0.007	372 of 392
	average		**2.16988**			**0.90997**			**17.0514**			**15.5165**			**36.9986**		
	1 SD (abs)		**0.00017**			**0.00004**			**0.0101**			**0.0089**			**0.0212**		
	1 SD (ppm)		78			40			594			572			572		
SRM610_23	90s, 1 µm/s, 100mJ, 6Hz, 60µm pit	6.4	2.16991	0.00014	388 of 396	0.90996	0.00004	384 of 396	17.042	0.003	379 of 396	15.509	0.003	381 of 396	36.979	0.007	382 of 396
SRM610_24	90s, 1 µm/s, 100mJ, 6Hz, 60µm pit	6.4	2.16952	0.00015	382 of 397	0.90992	0.00004	379 of 397	17.052	0.003	377 of 397	15.517	0.003	378 of 397	36.995	0.007	377 of 397
	average		**2.16971**			**0.90994**			**17.0471**			**15.5132**			**36.9870**		
	1 SD (abs)		**0.00027**			**0.00003**			**0.0076**			**0.0057**			**0.0110**		
	1 SD (ppm)		126			32			446			368			298		
SRM610_30	90s, 1 µm/s, 100mJ, 6Hz, 60µm pit	6.4	2.16997	0.00015	361 of 379	0.90998	0.00004	362 of 379	17.045	0.003	362 of 379	15.513	0.003	361 of 379	36.987	0.007	364 of 379
SRM610_31	90s, 1 µm/s, 100mJ, 6Hz, 60µm pit	6.4	2.17003	0.00015	369 of 384	0.91003	0.00004	366 of 384	17.045	0.003	367 of 384	15.511	0.003	367 of 384	36.987	0.007	365 of 384
	average		**2.17000**			**0.91000**			**17.0451**			**15.5119**			**36.9868**		
	1 SD (abs)		**0.00004**			**0.00004**			**0.0001**			**0.0010**			**0.0001**		
	1 SD (ppm)		20			41			5			65			2		
SRM610_32	90s, 1 µm/s, 100mJ, 6Hz, 60µm pit	6.3	2.17014	0.00014	382 of 399	0.91008	0.00004	381 of 399	17.048	0.003	380 of 399	15.515	0.003	380 of 399	36.996	0.007	379 of 399
SRM610_33	90s, 1 µm/s, 100mJ, 6Hz, 60µm pit	6.3	2.16976	0.00015	356 of 374	0.90996	0.00005	355 of 374	17.046	0.003	357 of 374	15.512	0.003	353 of 374	36.987	0.007	355 of 374
	average		**2.16995**			**0.91002**			**17.0472**			**15.5139**			**36.9915**		
	1 SD (abs)		**0.00027**			**0.00009**			**0.0014**			**0.0020**			**0.0065**		
	1 SD (ppm)		123			94			81			128			176		
Daily averages (August 23)			**2.16990**			**0.90998**			**17.05009**			**15.51575**			**36.99587**		
	1 SD (abs)		**0.00018**			**0.00005**			**0.00730**			**0.00618**			**0.01496**		
	1 SD (ppm)		81			52			428			398			404		
	1 SE (ppm)		24			16			129			120			122		
July 05, 2005	all: 90s, 1 µm/s, 100mJ, 6Hz, 60µm pit																
050705_SRM610_1	1.2 l/min He-flow	6.6	2.16968	0.00028	326 of 344	0.90997	0.00007	332 of 344	17.048	0.007	328 of 344	15.514	0.006	327 of 344	36.991	0.014	332 of 344
050705_SRM610_2	1.2 l/min He-flow	6.7	2.16934	0.00033	328 of 345	0.90992	0.00008	333 of 345	17.038	0.007	327 of 345	15.504	0.006	333 of 345	36.959	0.014	328 of 345
050705_SRM610_3	1.2 l/min He-flow	6.6	2.16992	0.00032	367 of 379	0.91007	0.00009	365 of 379	17.065	0.006	365 of 379	15.528	0.006	361 of 379	37.028	0.014	360 of 379
050705_SRM610_4	0.6 l/min He-flow	6.4	2.16964	0.00023	363 of 379	0.90990	0.00006	363 of 379	17.046	0.005	362 of 379	15.512	0.005	360 of 379	36.986	0.011	361 of 379
050705_SRM610_5	0.6 l/min He-flow	6.8	2.16918	0.00025	354 of 370	0.90982	0.00006	352 of 370	17.043	0.005	354 of 370	15.506	0.005	350 of 370	36.967	0.011	351 of 370
050705_SRM610_6	0.6 l/min He-flow	6.5	2.16897	0.00023	357 of 374	0.90975	0.00006	361 of 374	17.048	0.005	358 of 374	15.509	0.004	357 of 374	36.975	0.010	356 of 374
050705_SRM610_7	0.3 l/min He-flow	6.5	2.17003	0.00028	281 of 295	0.90999	0.00008	282 of 295	17.039	0.006	282 of 295	15.505	0.005	282 of 295	36.975	0.013	281 of 295
050705_SRM610_8	0.3 l/min He-flow	6.6	2.17045	0.00028	286 of 302	0.91008	0.00008	287 of 302	17.046	0.006	289 of 302	15.515	0.006	290 of 302	36.995	0.014	290 of 302
050705_SRM610_9	0.3 l/min He-flow	6.7	2.16949	0.00028	287 of 303	0.90990	0.00008	289 of 303	17.043	0.006	295 of 303	15.508	0.006	294 of 303	36.973	0.014	296 of 303
050705_SRM610_10	0.3 l/min He-flow; 5mm tubing	6.4	2.16922	0.00024	306 of 315	0.90977	0.00006	301 of 315	17.043	0.005	301 of 315	15.507	0.005	301 of 315	36.969	0.011	300 of 315
050705_SRM610_11	0.3 l/min He-flow; 5mm tubing	6.4	2.16996	0.00025	302 of 312	0.91003	0.00006	300 of 312	17.044	0.005	298 of 312	15.511	0.004	301 of 312	36.986	0.011	300 of 312
050705_SRM610_12	0.3 l/min He-flow; 5mm tubing	6.5	2.16936	0.00021	310 of 324	0.90995	0.00005	309 of 324	17.030	0.005	310 of 324	15.496	0.004	308 of 324	36.943	0.011	307 of 324
050705_SRM610_13	as shot 10 but nebulizer flow reduced to 1.3 l/mir	6.4	2.16963	0.00025	307 of 321	0.90999	0.00007	308 of 321	17.054	0.005	307 of 321	15.521	0.005	306 of 321	37.000	0.011	303 of 321
	average		**2.16961**			**0.90993**			**17.0452**			**15.5104**			**36.9806**		
	1 SD (abs)		**0.00041**			**0.00011**			**0.0083**			**0.0080**			**0.0211**		
	1 SD (ppm)		188			116			488			517			571		

July 06, 2005																
050706_SRM610_1	90s, 1 µm/s, 70mJ, 6Hz, 60µm pit, 0.6L He	6.4	2.16968	0.00025	373 of 386	0.90996	0.00006	368 of 386	17.054	0.006	369 of 386	15.518	0.005	367 of 386	36.994	0.012	370 of 386
050706_SRM610_2	90s, 1 µm/s, 70mJ, 6Hz, 60µm pit, 0.6L He	6.3	2.16936	0.00029	367 of 381	0.90985	0.00007	372 of 381	17.042	0.006	365 of 381	15.507	0.006	366 of 381	36.967	0.014	368 of 381
050706_SRM610_3	90s, 1 µm/s, 70mJ, 6Hz, 60µm pit, 0.6L He	6.4	2.16973	0.00027	352 of 372	0.90993	0.00007	352 of 372	17.060	0.006	354 of 372	15.523	0.006	353 of 372	37.014	0.013	352 of 372
	average		**2.16959**			**0.90992**			**17.0519**			**15.5159**			**36.9916**		
	1 SD (abs)		**0.00020**			**0.00006**			**0.0089**			**0.0082**			**0.0239**		
	1 SD (ppm)		92			63			521			530			646		
050706_SRM610_4	90s, 1 µm/s, 70mJ, 6Hz, 60µm pit, 0.6L He	6.4	2.16933	0.00034	355 of 372	0.90984	0.00008	359 of 372	17.066	0.008	357 of 372	15.530	0.008	356 of 372	37.025	0.019	360 of 372
050706_SRM610_5	90s, 1 µm/s, 70mJ, 6Hz, 60µm pit, 0.6L He	6.5	2.16943	0.00032	373 of 388	0.90974	0.00008	374 of 388	17.047	0.008	373 of 388	15.509	0.007	373 of 388	36.982	0.017	371 of 388
050706_SRM610_6	90s, 1 µm/s, 70mJ, 6Hz, 60µm pit, 0.6L He	6.4	2.16917	0.00033	357 of 375	0.90976	0.00008	356 of 375	17.047	0.008	357 of 375	15.509	0.007	362 of 375	36.978	0.016	358 of 375
	average		**2.16931**			**0.90978**			**17.0532**			**15.5158**			**36.9949**		
	1 SD (abs)		**0.00013**			**0.00005**			**0.0110**			**0.0121**			**0.0262**		
	1 SD (ppm)		61			57			647			781			708		
Daily average (July 06)			**2.16945**			**0.90985**			**17.053**			**15.516**			**36.993**		
	1 SD (abs)		**0.00022**			**0.00009**			**0.009**			**0.009**			**0.022**		
	1 SD (ppm)		100			98			527			597			608		
	1 SE (ppm)		41			40			215			244			248		
Nu Plasma grand average			**2.16956**			**0.90989**			**17.054**			**15.517**			**36.997**		
	1 SD (abs)		**0.00038**			**0.00010**			**0.011**			**0.010**			**0.024**		
	1 SD (ppm)		174			112			673			625			649		
	1 SE (ppm)		71			46			275			255			265		

Notes: Values in italics were rejected from the data base due to measured Pb/Tl intensity ratios exceeding 9 (explained in text)
1 SE abs refer to 1 standard error measurement uncertainties from the reported number of individual 0.2 s data readings (cycles)

Table A2: Synthetic fluid inclusion Pb isotope ratios acquired during this study, based on averages of isotope ratios calculated from 0.2 s data readouts and not corrected for amplifier response

	FI chip number	FI size (µm)	Ablation quality	$^{208}Pb/^{206}Pb$ final	1 SE abs	# of readings	$^{207}Pb/^{206}Pb$ final	1 SE abs	# of readings	$^{206}Pb/^{204}Pb$ final	1 SE abs	# of readings	$^{207}Pb/^{204}Pb$ final	1 SE abs	# of readings	$^{208}Pb/^{204}Pb$ final	1 SE abs	# of readings
SRM 981 reference values (Baker et al., 2004)				2.1678			0.91489			16.942			15.500			36.725		
NU Plasma 1700																		
August 30, 2005																		
Pb-Tl_FI-1_Aug30-05	A2	30	+++	2.1688	0.0010	51 of 52	0.91472	0.00030	50 of 52	16.978	0.017	49 of 52	15.526	0.018	49 of 52	36.795	0.044	49 of 52
Pb-Tl_FI-2_Aug30-05	A2	50	+++	2.1653	0.0015	60 of 64	0.91391	0.00038	60 of 64	16.941	0.009	62 of 64	15.483	0.011	62 of 64	36.682	0.038	60 of 64
Pb-Tl_FI-3_Aug30-05	A3	50	++(+)	2.1666	0.0007	118 of 123	0.91458	0.00020	118 of 123	16.937	0.007	115 of 123	15.495	0.007	116 of 123	36.709	0.019	117 of 123
Pb-Tl_FI-4_Aug30-05	A3	50	++	2.1665	0.0008	102 of 107	0.91451	0.00022	100 of 107	16.932	0.006	103 of 107	15.489	0.006	102 of 107	36.693	0.018	101 of 107
Pb-Tl_FI-5_Aug30-05	A3	35	+++	2.1728	0.0019	41 of 43	0.91590	0.00045	41 of 43	16.840	0.013	40 of 43	15.433	0.014	41 of 43	36.586	0.043	40 of 43
Pb-Tl_FI-6_Aug30-05	A3	50	++	2.1697	0.0013	66 of 68	0.91539	0.00032	67 of 68	16.908	0.008	65 of 68	15.475	0.010	64 of 68	36.674	0.029	67 of 68
Pb-Tl_FI-7_Aug30-05	A3	50	++	2.1668	0.0008	89 of 95	0.91452	0.00023	89 of 95	16.923	0.006	88 of 95	15.478	0.006	88 of 95	36.673	0.019	89 of 95
Pb-Tl_FI-8_Aug30-05	*A3*	*40*	*exploded*	*2.1635*	*0.0035*	*40 of 41*	*0.91389*	*0.00084*	*40 of 41*	*16.923*	*0.023*	*39 of 41*	*15.469*	*0.028*	*39 of 41*	*36.626*	*0.089*	*39 of 41*
			average	2.1681			0.91479			16.923			15.483			36.687		
			2stdev	0.0051			0.0013			0.0843			0.0556			0.1230		
			(%)	0.24			0.14			0.50			0.36			0.34		
NU Plasma																		
August 23, 2003																		
FI_Pb_Tl_1	B1	20	+++	2.1689	0.0033	35 of 37	0.91481	0.00159	37 of 37	16.867	0.358	36 of 37	15.423	0.338	36 of 37	36.562	0.783	36 of 37
FI_Pb_Tl_2	B1	40	+++	2.1659	0.0013	49 of 51	0.91405	0.00056	47 of 51	16.773	0.109	48 of 51	15.298	0.093	47 of 51	36.341	0.238	48 of 51
FI_Pb_Tl_3	B1	80	+++	2.1616	0.0021	26 of 28	0.91386	0.00144	26 of 28	16.965	0.066	27 of 28	15.470	0.060	27 of 28	36.671	0.153	27 of 28
FI_Pb_Tl_4	*B1*	*40*	*exploded*	*2.1591*	*0.0030*	*25 of 26*	*0.90986*	*0.00186*	*25 of 26*	*16.926*	*0.094*	*24 of 26*	*15.428*	*0.089*	*24 of 26*	*36.559*	*0.217*	*24 of 26*
FI_Pb_Tl_5	A2	90	+++	2.1652	0.0005	135 of 143	0.91357	0.00032	133 of 143	16.966	0.008	137 of 143	15.500	0.007	134 of 143	36.732	0.020	137 of 143
FI_Pb_Tl_6	A2	90	+++	2.1663	0.0004	205 of 221	0.91393	0.00019	205 of 221	16.974	0.005	213 of 221	15.520	0.004	208 of 221	36.774	0.012	214 of 221
FI_Pb_Tl_7	A2	60	+++	2.1657	0.0004	137 of 144	0.91377	0.00018	137 of 144	16.970	0.009	139 of 144	15.507	0.009	136 of 144	36.752	0.022	137 of 144
FI_Pb_Tl_8	A2	50	+++	2.1637	0.0008	30 of 32	0.91387	0.00047	31 of 32	16.995	0.022	31 of 32	15.498	0.018	31 of 32	36.758	0.052	31 of 32
			average	2.1653			0.91398			16.930			15.459			36.656		
			2stdev	0.0061			0.0030			0.1489			0.1460			0.2984		
			(%)	0.28			0.33			0.88			0.94			0.81		
August 23, 2003																		
FI_Pb_1	C3	20	+++	2.1652	0.0019	9 of 9	0.91495	0.00151	8 of 9	16.929	0.058	8 of 9	15.540	0.099	9 of 9	36.806	0.199	8 of 9
FI_Pb_2	C3	25	+++	2.1639	0.0012	34 of 36	0.91286	0.00069	33 of 36	16.995	0.278	35 of 36	15.424	0.237	34 of 36	36.785	0.600	35 of 36
FI_Pb_3	C1	20	++	2.1648	0.0009	18 of 18	0.91417	0.00111	17 of 18	16.974	0.022	17 of 18	15.502	0.021	17 of 18	36.753	0.043	16 of 18
FI_Pb_4	*C1*	*60*	*exploded*	*2.1642*	*0.0024*	*17 of 17*	*0.91102*	*0.00309*	*16 of 17*	*17.079*	*0.119*	*16 of 17*	*15.518*	*0.109*	*17 of 17*	*36.943*	*0.246*	*16 of 17*
FI_Pb_5	C1	50	++	2.1664	0.0005	144 of 152	0.91476	0.00027	146 of 152	17.071	0.074	145 of 152	15.617	0.068	145 of 152	36.984	0.157	146 of 152
FI_Pb_6	C1	25	+++	2.1650	0.0015	12 of 12	0.91456	0.00150	11 of 12	16.889	0.069	12 of 12	15.403	0.034	11 of 12	36.565	0.138	12 of 12
FI_Pb_7	C1	45	++	2.1669	0.0007	28 of 29	0.91430	0.00054	29 of 29	16.977	0.071	27 of 29	15.539	0.062	27 of 29	36.789	0.148	27 of 29
			average	2.1654			0.91427			16.973			15.504			36.780		
			2stdev	0.0022			0.0015			0.1231			0.1599			0.2675		
			(%)	0.10			0.16			0.73			1.03			0.73		

Notes: "Ablation quality" refers to the quality of fluid inclusion ablation as observed on monitor screen (+++ = excellent, ++ = acceptable, + = poor)
1 SE abs refers to the 1 standard deviation of the mean calculated from n readings
Values in italics were rejected from the data set due to uncontrolled fluid inclusion ablation ("exploded")